



# $\beta$ -Hydroxybutyrate enhances chondrocyte mitophagy and reduces cartilage degeneration in osteoarthritis via the HCAR2/AMPK/PINK1/Parkin pathway

Huangming Zhuang | Xunshan Ren | Yuelong Zhang | Huajie Li | Panghu Zhou 

Department of Orthopedics, Renmin Hospital of Wuhan University, Wuhan, China

#### Correspondence

Panghu Zhou, Department of Orthopedics, Renmin Hospital of Wuhan University, Wuhan 430060, China.  
Email: [zhoupanghu@126.com](mailto:zhoupanghu@126.com)

#### Funding information

National Natural Science Foundation of China, Grant/Award Number: 82372489; Hubei Medical Youth Tip-Top Talent to Panghu Zhou, Grant/Award Number: CZ2024020005-11; Fundamental Research Funds for the Central Universities, Grant/Award Number: 2042023kf0224; Wuhan University Education and Development Foundation, Grant/Award Number: 2002330; Cross-Innovation Talent Program of Renmin Hospital of Wuhan University, Grant/Award Number: JCRCFZ-2022-019

## Abstract

Osteoarthritis (OA) is widely recognized as the prevailing joint disease associated with aging. The ketogenic diet (KD) has been postulated to impede the advancement of various inflammatory ailments.  $\beta$ -Hydroxybutyrate ( $\beta$ OHB), a prominent constituent of ketone bodies, has recently been proposed to possess crucial signaling capabilities. In this study, we propose to explore the role and mechanism of  $\beta$ OHB in OA. Tissue staining and inflammatory factor assay were employed to evaluate the impacts of KD and  $\beta$ OHB on OA rats. The oxidative stress conditions in chondrocytes were induced using tert-butyl hydroperoxide (TBHP). The mechanisms were determined using the siRNA of hydroxycarboxylic acid receptor 2 (HCAR2), the antagonist of adenosine monophosphate-activated protein kinase (AMPK), and the inhibitor of mitophagy. The administration of KD demonstrated a reduction in pathological damage to cartilage, as well as a decrease in plasma levels of inflammatory factors. Furthermore, it resulted in an increase in the concentration of  $\beta$ OHB in the blood and synovial fluid. In vitro experiments showed that  $\beta$ OHB facilitated mitophagy and adenosine triphosphate production. Besides,  $\beta$ OHB mitigated chondrocyte senescence, inflammatory factors secretion, extracellular matrix degradation, and apoptosis induced by TBHP. Subsequent investigations indicated that the protective effects of  $\beta$ OHB were no longer observed following the knockdown of HCAR2, the antagonist of AMPK, or the inhibitor of mitophagy. Moreover, in vivo studies suggested that  $\beta$ OHB played a protective role by targeting the HCAR2-AMPK-PINK1 axis. In conclusion,  $\beta$ OHB enhanced

**Abbreviations:**  $\beta$ OHB,  $\beta$ -Hydroxybutyrate;  $\Delta\psi_m$ , mitochondrial membrane potential; ACLT, anterior cruciate ligament transection; AMPK, adenosine monophosphate-activated protein kinase; ATP, adenosine triphosphate; BAX, BCL2-associated X protein; BCL2, B-cell lymphoma 2; CAT, catalase; CCK-8, cell counting kit-8; cleaved PARP-1, cleaved polyADP-ribose polymerase 1; Col2a1, collagen type II alpha 1; H&E, hematoxylin-eosin; HCAR2, hydroxycarboxylic acid receptor 2; IL-6, interleukin-6; iNOS, inducible nitric oxide synthase; KD, ketogenic diet; LC3B, microtubule-associated protein 1 light chain 3 beta; Mdivi-1, mitochondrial division inhibitor-1; MMP13, matrix metalloproteinase 13; OA, osteoarthritis; OARSI, Osteoarthritis Research Society International; OCR, Oxygen consumption rate; P16, cyclin-dependent kinase 4 inhibitor; P21, cyclin-dependent kinase inhibitor 1A; p-AMPK, phospho-AMPK $\alpha$  Thr172; PBS, phosphate-buffered saline; PGE2, prostaglandin E2; PINK1, PTEN induced putative kinase 1; pNA, p-nitroaniline; p-Parkin, phospho-Parkin-Ser65; p-Ub, phospho-Ubiquitin-Ser65; RNS, reactive nitrogen species; ROS, reactive oxygen species; RT-qPCR, reverse transcription-quantitative polymerase chain reaction; SASP, senescence-associated secretory phenotype; SA- $\beta$ -Gal, senescence-associated  $\beta$ -galactosidase; SD, standard diet; SOD1, superoxide dismutase 1; TBHP, tert-butyl hydroperoxide; TNF- $\alpha$ , tumor necrosis factor- $\alpha$ ; TOMM20, translocase of outer mitochondrial membrane 20.

Huangming Zhuang and Xunshan Ren contributed equally to this work.

This is an open access article under the terms of the [Creative Commons Attribution](#) License, which permits use, distribution and reproduction in any medium, provided the original work is properly cited.

© 2024 The Author(s). *Aging Cell* published by the Anatomical Society and John Wiley & Sons Ltd.



chondrocyte mitophagy through the HCAR2/AMPK/PINK1/Parkin pathway, offering a potential therapeutic approach for the treatment of OA.

#### KEY WORDS

hydroxycarboxylic acid receptor 2, mitophagy, osteoarthritis, senescence,  $\beta$ -Hydroxybutyrate

## 1 | INTRODUCTION

Osteoarthritis (OA) affects approximately 25% of individuals aged 60 and above (Hunter & Bierma-Zeinstra, 2019). The rising incidence of OA can be attributed to factors such as obesity and the aging population, leading to a significant societal and familial burden (O'Neill et al., 2018). In cases of advanced OA, arthroplasty is often necessary to restore joint function due to the limited efficacy of available treatments (Bannuru et al., 2019). The pathogenesis of OA is multifaceted, involving various mechanisms such as chondrocyte senescence, pro-inflammatory cytokine release, oxidative stress injury, apoptosis, impaired mitochondrial energy metabolism, and dysregulated protein metabolism (Goutas et al., 2018). These intricate etiologies interact synergistically to result in common clinical manifestations ultimately. Mitophagy is vital in maintaining mitochondrial quality control and homeostasis *in vivo* (Sun et al., 2021). Impairment of mitophagy leads to the gradual buildup of defective mitochondria, ultimately causing chondrocyte apoptosis, extracellular matrix degradation, and cartilage degeneration (Ansari et al., 2018).

Chondrocytes, the sole resident cells in articular cartilage, maintain cartilage homeostasis through the secretion of aggrecan and collagen type II (Zhang et al., 2023). Age is a well-established independent risk factor for OA, characterized by the accumulation of senescent chondrocytes (Chen et al., 2021). The cell cycle is irreversibly arrested during chondrocyte senescence, and the senescence-associated secretory phenotype (SASP) emerges (Huang et al., 2022). The activation of SASP factors induces cellular inflammatory responses, oxidative stress, and cartilage matrix degradation, indicating that targeting chondrocyte senescence is crucial for therapeutic interventions in OA (Lopez-Otin et al., 2023).

In recent times, there has been a growing focus on the impact of dietary modifications and the resulting metabolic alterations on chondrocyte dysfunction (Nasui et al., 2022; Zheng et al., 2021). Ketogenic diet (KD), which follow a high-fat and low-carbohydrate diet, has been found to profoundly alter human metabolomes, particularly by increasing the levels of circulating ketone bodies (Effinger et al., 2023). The KD has demonstrated immunomodulatory properties and has shown potential in alleviating symptoms associated with several chronic ailments. However, there is still a need for further investigation regarding the therapeutic role and mechanisms of KD in OA (Abboud et al., 2021).  $\beta$ -Hydroxybutyrate ( $\beta$ OHB) is one of the most significant components of ketone bodies (Sharma & Ramanathan, 2020). The metabolic analysis of knee synovial fluid in OA patients revealed a decrease in  $\beta$ OHB concentration, which exhibited a negative correlation with collagen levels (Mickiewicz et al., 2015). Recent research has highlighted the

role of ketone bodies as both energy carriers and signaling molecules (Newman & Verdin, 2014). Specifically, it has been demonstrated that  $\beta$ OHB downregulated the production of inflammatory cytokines in microglia stimulated by lipopolysaccharide (Fu et al., 2014), inhibited the inflammatory activation of bone marrow macrophages (Youn et al., 2015), and mitigated myocardial oxidative stress in septic cardiomyopathy (Ji et al., 2022). Moreover, previous clinical investigations have demonstrated the favorable safety profile of exogenous supplementation of  $\beta$ OHB (Stefan et al., 2021). Considering the modulatory effects of  $\beta$ OHB on energy metabolism, inflammatory reactions and oxidative stress, exploring its potential therapeutic applications in OA is valuable. Hydroxycarboxylic acid receptor 2 (HCAR2), also referred to as G protein-coupled receptor 109a (GPR109a), serves as a significant endogenous receptor for  $\beta$ OHB (Dmitrieva-Posocco et al., 2022; Zhao et al., 2023). Adenosine monophosphate-activated protein kinase (AMPK), a highly conserved master regulator of cellular energy metabolism, can be activated through the supplementation of  $\beta$ OHB (Carretta et al., 2020; Hardie et al., 2012). Consequently, we postulated that the activation of HCAR2 and AMPK may be intricately linked to the mechanism of action of  $\beta$ OHB.

This study aimed to evaluate the capacity and mechanism of  $\beta$ OHB in mitigating oxidative stress, mitochondrial dysfunction, cellular senescence, and apoptosis induced by tert-butyl hydroperoxide (TBHP) *in vitro*. Additionally, the effects of KD and  $\beta$ OHB were examined in an OA rat model.

## 2 | METHODS

### 2.1 | Ethics statement

All experiments involving animals were conducted according to the ethical policies and procedures approved by the Laboratory Animal Welfare & Ethics Committee of the Renmin Hospital of Wuhan University (Approval No: 20220103A).

### 2.2 | Cell culture

Primary chondrocytes were obtained from 8-week-old Wistar rats. In brief, an overdose of pentobarbital intraperitoneally was administered to the rats, followed by immersion in 75% ethanol for 10 min. Subsequently, knee cartilage was aseptically isolated and fragmented into smaller pieces. After 30 min of enzymatic digestion with 0.25% trypsin, the cartilage fragments were subjected to 8 h



of enzymatic digestion with 0.1% collagenase II. Chondrocytes were harvested and cultured in media containing 10% fetal bovine serum. Our study utilized only second-generation chondrocytes to preserve chondrocyte phenotypic characteristics.

### 2.3 | Cell viability assay

For measuring the cytotoxicity of  $\beta$ OHB (S33155, Shyuanye) and TBHP (B106035, Aladdin), a cell counting kit-8 (CCK-8, G4103, Servicebio) was used. Cells were cultured at a density of  $5 \times 10^3$ /well in 96-well plates. Different concentrations of  $\beta$ OHB (0.5, 1, 2, 4, and 8 mM) or TBHP (0, 5, 10, 15, 20, and 25  $\mu$ M) were added. The absorbance of each concentration was measured at 24, 48, and 72 h using a microplate reader.

### 2.4 | Senescence-associated $\beta$ -galactosidase (SA- $\beta$ -Gal) staining and Alcian blue staining

Following a 72-h treatment of TBHP and  $\beta$ OHB, chondrocytes were cultured with  $\beta$ -galactosidase Staining Fixative and then stained with the senescence  $\beta$ -galactosidase Staining Solution (C0602, Beyotime) overnight at 37°C. For Alcian blue staining, chondrocytes were incubated with Alcian blue reagent (BH0004, Powerful Biology) for 1 h. Subsequently, the cells were photographed under a light microscope.

### 2.5 | Reverse transcription-quantitative polymerase chain reaction (RT-qPCR)

The intervention time for TBHP and  $\beta$ OHB in this study was 48 h, unless otherwise specified. The extraction of total RNA was performed using TRIzol® Reagent. Complementary DNA synthesis was performed utilizing the mRNA Reverse Transcription Kit (AG11728, Accurate Biotech). The RT-qPCR was undertaken on LightCycler® 480 Software (Roche, Swiss Confederation) using 2  $\times$  SYBR Green qPCR Mix Kits (G3320, Servicebio). The primer sequences utilized in this investigation are provided in Table 1. The relative mRNA expression was normalized to  $\beta$ -actin using the  $2^{-\Delta\Delta Ct}$  method.

### 2.6 | Immunofluorescence

Chondrocytes underwent a series of procedures, including washing with phosphate-buffered saline (PBS), fixation with 4% paraformaldehyde, and incubation with 3% bovine serum albumin for 30 min at room temperature. Subsequently, cells were incubated with primary antibodies against collagen type II alpha 1 (Col2a1, 1:200, GB11021, Servicebio), Aggrecan (1:200, GB11373, Servicebio), translocase of outer mitochondrial membrane 20 (TOMM20, 1:250, ab186734, Abcam), PTEN induced putative kinase 1 (PINK1, 1:50, A7131, Abclonal), and microtubule-associated protein 1 light chain 3 beta

TABLE 1 Primer sequences used in this study.

Gene name	F/R	Sequences 5'-3'
P16	F	GAGGACCCCACCAACCTCTC
	R	ATACCGCAAATACCGCACGA
P21	F	AGCAGTTGAGCCGCGATTG
	R	ACCCAGGGCTCAGGTAGATCTTG
Aggrecan	F	AGTGACCCATCTGCTTACCTTG
	R	CTGCATCTATGTCGGAGGTAGTG
Col2a1	F	GACTGTGCCCTCGGAAGAA
	R	CTGGACGTTAGCGGTGTT
IL6	F	AAATCTGCTCTGGTCTTC
	R	AGGGTTTCAGTATTGCTC
MMP13	F	GCCACCTTCTTCTGTTGAGTTG
	R	GACTTCTTCAGGATTCCCGCA
BAX	F	TTTTTGCTACAGGGTTTC
	R	TTGTTGTCAGGTTCATCG
BCL2	F	GAGAGCGTCAACAGGGAG
	R	GCCAGGAGAAATCAAACA
CAT	F	CAGATGTGAAGCGCTAACAGT
	R	GGGTGGACGTCAGTGAATTC
SOD1	F	GCAGAAGGCAAGCGGTGAAC
	R	CCAGGTCTCCAACATGCCTC
$\beta$ -Actin	F	TGCTATGTTGCCCTAGACTTCG
	R	GTTGGCATAGAGGTCTTACGG

Abbreviations: F, Forward; R, Reverse.

(LC3B, 1:100, A19665, Abclonal) overnight at 4°C, followed by incubation with secondary antibodies for 1 h. The nuclei were stained with 4',6-diamidino-2-phenylindole, and the fluorescence intensity was observed using a fluorescence microscope. To quantify the immunostaining, ROS, and JC-1 staining images, images of the same size were randomly selected with the same exposure time. The fluorescence intensity of the images was converted to grayscale and evaluated using the ImageJ software (version 1.8) at the same threshold.

### 2.7 | Western blotting

Total protein was extracted using a lysis buffer containing phosphorylated protease inhibitors. A BCA Protein Detection Kit (W041-1-1, NJJCBIO) was used to determine the protein concentration. Protein separation was accomplished by sodium dodecyl sulfate-polyacrylamide gel electrophoresis and transferred onto 0.45  $\mu$ M polyvinylidene difluoride membranes. The membranes were incubated overnight at 4°C with primary antibodies targeting cyclin-dependent kinase 4 inhibitor (P16, 1:500, PA1210, Abmart), cyclin-dependent kinase inhibitor 1A (P21, 1:1000, PA9426, Abmart), inducible nitric oxide synthase (iNOS, 1:1000, A14031, Abclonal), IL6 (1:1000, TD6087, Abmart), matrix metalloproteinase 13 (MMP13, 1:1000, 18165-1, Proteintech), Cleaved



Caspase-3 (1:1000, #9661, Cell Signaling Technology), B-cell lymphoma 2 (BCL2, 1:1000, ab196495, Abcam), BCL2-associated X Protein (BAX, 1:1000, 50599-2, Proteintech), Catalase (CAT, 1:1000, A11777, Abclonal), superoxide dismutase 1 (SOD1, 1:5000, ab13498, Abcam), PINK1 (1:1000, A7131, Abclonal), Parkin (1:500, A0968, Abclonal), phospho-Parkin-Ser65 (p-Parkin, 1:500, PA5-114616, Thermo Fisher), P62/SQSTM1 (1:5000, ab109012, Abcam), LC3B (1:500, A19665, Abclonal), phospho-Ubiquitin-Ser65 (p-Ub, 1:500, CPA5761, Cohesion), cleaved polyADP-ribose polymerase 1 (cleaved PARP-1, 44-698G, Thermo Fisher), phospho-AMPK $\alpha$  Thr172 (p-AMPK, 1:1000, 2535, Cell Signaling Tech), anti-AMPK $\alpha$  (1:2000, 10929-2-AP, Proteintech), HCAR2 (1:1000, A15611, ABclonal, China), and  $\beta$ -actin (1:3000, GB11001, Servicebio). Subsequently, the strips were incubated with a secondary antibody for 1 h. The protein immunoreactivity was then detected using the Bio-Rad scanner and semi-quantified by ImageJ software (version 1.8).

## 2.8 | Caspase 3 activity assay

Caspase 3 activity was determined using the Caspase 3 Activity Assay Kit (C1115, Beyotime). The Caspase 3 Activity Assay Kit employs the enzymatic activity of caspase 3 on the substrate acetyl-Asp-Glu-Val-Asp p-nitroanilide to quantify caspase 3 activity by measuring the concentration of the product, p-nitroaniline (pNA), through absorbance readings. Chondrocytes were collected with trypsin and resuspended in cell culture medium. Then cells were washed with PBS prior to lysis using a ratio of 100  $\mu$ L of lysate per 2 million cells. The lysate was then incubated on ice for 15 min and subsequently centrifuged at 4°C at 16,000g for 10 min. The protein concentration in each sample was determined using the Bradford method to standardize the protein concentration to 3 mg/mL. Subsequently, the protein samples were combined with assay buffer and exposed to Ac-DEVD-pNA (2 mM) for 120 min at 37°C. The absorbance resulting from caspase 3-mediated production of pNA was quantified at 405 nm using a microplate reader.

## 2.9 | Determination of reactive oxygen species (ROS) in chondrocytes and mitochondria

The ROS assay kit (G1706, Servicebio) was used to detect intracellular ROS levels. Briefly, chondrocytes were incubated with DCFH-DA at a ratio of 1:1000 in serum-free medium for 30 min at 37°C. Following this incubation period, chondrocytes were washed with serum-free medium and observed utilizing a fluorescence microscope.

The mitochondria ROS was measured by the Mitochondrial Reactive Oxygen Species Assay Kit (BB-46091, Bestbio). The mitochondrial ROS probe is able to permeate the cell membrane and specifically target chloromethyl functional groups within the mitochondria. Once inside the mitochondria, the probe undergoes rapid oxidation by ROS, resulting in the emission of red fluorescence that

allows for visualization of the mitochondria within live cells. In short, the culture medium was removed and replaced with a solution containing the mitochondrial ROS probe at 37°C, and the cells were then incubated under light protection for 30 min. Subsequently, the cell nuclei were stained with DAPI and photographed under a laser confocal microscope.

## 2.10 | Flow cytometry assay

The apoptosis ratio of each respective group was determined using the Apoptosis Assay Kit (40302ES, YEASEN) with a flow cytometer (Beckman Coulter, America). Briefly, a total of 10<sup>5</sup> chondrocytes were collected using ethylenediaminetetraacetic acid-free trypsin, washed twice with pre-cooled PBS, and then resuspended in 100  $\mu$ L of 1× Binding Buffer. The cells were subsequently incubated with 5  $\mu$ L Annexin V-FITC and 10  $\mu$ L PI staining solution in the dark at room temperature for 15 min. Following incubation, 400  $\mu$ L of 1× Binding Buffer was added to the samples, which were then analyzed using a flow cytometer within 1 h.

Reactive nitrogen species (RNS) refers to the interaction of iNOS with various compounds, including ROS, resulting in the production of highly oxidizing radicals and nitro compounds such as HOONO (Davies et al., 2008). The presence of RNS in cells was determined utilizing the Reactive Nitrogen Assay Kit (BB-462112, Bestbio). According to the experimental protocol, cells were washed with PBS and then exposed to a working solution of RNS probe staining at 37°C. After a 30-min incubation period shielded from light, any surplus probe that was not taken up by the cells was eliminated through PBS washing, and subsequently, 200  $\mu$ L of Hanks' Balanced Salt Solution buffer was added for analysis using a flow cytometer (Beckman Coulter, America).

## 2.11 | JC-1 mitochondrial membrane potential ( $\Delta\psi_m$ ) assay

JC-1 (C2003S, Beyotime), a cationic carbocyanine dye, exhibits aggregation and localization towards mitochondria. In normal state, JC-1 predominantly exists as polymers and exhibits red fluorescence. However, during early apoptosis, the decrease in  $\Delta\psi_m$  leads to a shift in JC-1 towards monomers, resulting in green fluorescence. The chondrocytes were cultured in six-well plates until reaching a density of 100,000 cells per well. The JC-1 staining working solution was diluted in accordance with the recommended ratio of 1 mL of JC-1 staining buffer for every 5  $\mu$ L of JC-1 (200×), as per the instructions provided by the reagent vendor. Following the washing of cells with PBS, a mixture of 1 mL of cell culture medium and an equal volume of 1 mL of the JC-1 staining working solution was added, thoroughly mixed, and incubated in a cell incubator at 37°C for 20 min. After the incubation period, the supernatant was removed and the cells were washed twice with JC-1 staining buffer. Subsequently, 2 mL of cell culture solution

was added. The randomly selected fields of view were observed and photographed under a fluorescence microscope.

## 2.12 | Comet assay

DNA Damage Comet Assay Kit (C2041S, Beyotime) was used to assess DNA damage in cells. A 1% normal melting point agarose gel and a 0.7% low melting point agarose gel were prepared following the guidelines provided by the reagent vendor. Subsequently, the gels were cooled in a water bath and made ready for use. Chondrocytes were washed thrice with PBS, digested with trypsin, and centrifuged to gather the cells. A 30 $\mu$ L aliquot of 1% normal melting point agarose gel, previously heated to 45°C, was applied to a slide, covered with a coverslip, and allowed to solidify at 4°C for 10 min. The coverslip was then gently removed. Subsequently, 10 $\mu$ L of cells were thoroughly mixed with 75 $\mu$ L of pre-warmed 0.7% low melting point agarose, and 70 $\mu$ L droplets were swiftly aspirated and added to the initial gel layer. The mixture was evenly spread with a pipette tip and left at 4°C for 10 min to solidify. The lysis solution was prepared by combining Lysis Buffer with DMSO in a 9:1 ratio, and the cells on the slides were lysed at 4°C for 2 h. Following the rinsing with PBS, the slides were subsequently immersed in electrophoresis buffer for a duration of 40 min at room temperature. This step was undertaken to facilitate the denaturation of DNA double strands within the cellular material under alkaline conditions, thereby enabling the fragmented DNA molecules to migrate efficiently within the electric field. The electrophoresis process was conducted at a modest voltage of 25 V within an ice bath environment, shielded from exposure to light. Following electrophoresis, the slides were immersed in a neutral buffer at 4°C, then the buffer was removed and approximately 20 $\mu$ L of propidium iodide solution was added drop by drop to the slides. The slides were then stained for 10–20 min in the absence of light. Subsequently, the slides were rinsed in ultrapure water, observed and photographed under a fluorescence microscope. Approximately 25 cells were randomly chosen from each sample, and the percentage of Tail DNA content (i.e., tail DNA intensity/cell DNA intensity) was determined.

## 2.13 | Oxygen consumption rate (OCR) and adenosine triphosphate (ATP) detection by seahorse

Mitochondrial bioenergetics in chondrocytes were assessed using Seahorse Bioscience Extracellular Flux Analyzers (XFe24, Agilent, USA) and Seahorse Bioscience Cell Mito Stress Test Kit (# 103015-100, Agilent). Following preparation of background-corrected wells on the XF24 cell culture plate, 100 $\mu$ L of chondrocytes were seeded into the remaining wells at a density of 50,000 cells per well. After allowing the cells to adhere to the plate, 150 $\mu$ L of growth medium was added to achieve a uniform monolayer of cells. Once the cell confluence reached 50%, interventions were carried out based on the experimental design.

One day prior to the experiment, 1 mL of XF Calibrant was added to each well in the hydrated plate to submerge the sensor cartridge in the calibrant. The probe plate device was then hydrated overnight in a 37°C CO<sub>2</sub>-free cell incubator. On the day of the assay, cells were incubated for 1 h in a CO<sub>2</sub>-free incubator using DMEM Medium containing 10 mM glucose, 2 mM glutamine, and 1 mM pyruvate. Then, 1.5  $\mu$ M Oligomycin, 2.0  $\mu$ M FCCP, and 0.5  $\mu$ M rotenone/antimycin A were sequentially added to the dosing wells of the probe plate. Subsequently, the probe plate and cell plate were placed into the instrument, and the XF Cell Mito Stress Test Kit in Wave Desktop 2.6 software was utilized as a reference. After measurement, the plates were extracted, 20 $\mu$ L of RIPA buffer was introduced, and the protein concentration was determined using the BCA assay. Subsequently, the OCR measurement was standardized to the overall protein content. Basal respiration, maximal respiration, spare respiration capacity, nonmitochondrial respiration, and ATP production were calculated by consulting the formula provided on the official website of the Agilent XF Assay Learning Center (<https://www.agilent.com.cn/en/product/cell-analysis/how-to-run-an-assay>).

## 2.14 | Transmission electron microscopy

To observe mitochondria, chondrocytes were collected through centrifugation at 800 rpm for 3 min, followed by fixation with 2.5% glutaraldehyde twice for 30 min each, and subsequent treatment with 1% osmium tetroxide for 2 h. After dehydration, infiltration, embedding, sectioning, and staining, transmission electron microscopy (Hitachi, Japan) was employed to visualize the mitochondria. In conducting a morphometric analysis of mitochondrial cristae, measurements of cristae perimeter and density were obtained utilizing the ImageJ Multimeasure plug-in. Mitochondria were then categorized based on the abundance of cristae, ranging from low to high (Balsa et al., 2019). Subsequently, percentage damaged mitochondria and mitophagy events were quantified.

## 2.15 | Knockdown by siRNA

Chondrocytes were transfected with siRNA HCAR2 or siRNA scramble using Lipofectamine 3000 transfection reagent (Invitrogen, America) and Opti-MEM (Invitrogen, America). The transfection mixture was added dropwise to the medium containing serum and incubated at 37°C with 5% CO<sub>2</sub> for 8 h. Subsequently, the transfection reagent medium was replaced with a standard cell growth medium. After confirming the transfection efficiency of siRNA HCAR2 through western blotting, subsequent experiments were conducted.

## 2.16 | Rat OA model construction

A total of seventy-five 8-week-old Wistar rats were included in this study. Anterior cruciate ligament transection (ACLT) was conducted



in a sterile environment and sustained for 2 weeks to establish an OA model (Jin et al., 2022).

In the initial phase of animal experimentation, 20 rats were randomly allocated into 4 groups to examine the impact of SD and a KD on the progression of OA: the sham + SD group, the sham + KD group, the ACLT + SD group, and the ACLT + KD group. The nutritional composition of the SD and KD can be found in Table 2. The  $\beta$ OHB Colorimetric Assay Kit (E-BC-K785-M, Elabscience) operates on the principle that  $\beta$ OHB is oxidized by  $\beta$ OHB dehydrogenase, concurrently reducing  $\text{NAD}^+$  to  $\text{NADH}$ . This reaction subsequently induces a color change in WST-8 to an orange-yellow hue through the action of hydrogen-transferring substances. The  $\beta$ OHB concentration can be quantified by measuring the absorbance at 450 nm, which is directly proportional to the  $\beta$ OHB content. In brief, samples were collected and subjected to centrifugation in a 50 kDa ultrafiltration tube at 10,000 $\times g$  for 15 min. Subsequently, 10  $\mu\text{L}$  of each sample, along with varying concentrations of standards, were added to the respective wells of the enzyme assay plate. Fifty microliter of Enzyme Reagent was added to each well, followed by incubation at 37°C for 10 min. Subsequently, 160  $\mu\text{L}$  of chromogenic agent was added, and the mixture was incubated at 37°C for an additional 30 min. The optical density value of each well was then measured at 450 nm using a microplate reader. After 8 weeks, the rats were euthanized through cervical dislocation while under anesthesia. The concentration of tumor necrosis factor- $\alpha$  (TNF- $\alpha$ , ER1393, FineTest), interleukin-6 (IL-6, E-EL-R0015c, Elabscience), and prostaglandin E2 (PGE2, ER1800, FineTest) were determined using enzyme-linked immuno sorbent assay kits, following the guidelines provided by the manufacturers. The concentration of nitric oxide was quantified using the Griess reagent (Beyotime, S0024). After 3 days of fixation with a 4% paraformaldehyde solution, the articular cartilage underwent decalcification through immersion in a 10% ethylenediaminetetraacetic acid solution and subsequent incubation for 30 days. The decalcifying solution was replaced every 3 days. Subsequently, the samples were subjected to dehydration in ethanol and embedding in paraffin wax.

In the subsequent round of animal experiments, an additional 25 rats were randomly assigned to 5 groups: sham group, ACLT group, ACLT + 50 mg/kg  $\beta$ OHB group, ACLT + 100 mg/kg  $\beta$ OHB group, and

ACLT + 200 mg/kg  $\beta$ OHB group. A study on atherosclerosis found that  $\beta$ OHB significantly reduced serum levels of inflammatory factors, mainly when administered at a dosage of 100 mg/kg/day through intragastric administration (Zhang et al., 2021). Therefore, in the ACLT +  $\beta$ OHB group, rats were injected with 50, 100, or 200 mg/kg of  $\beta$ OHB daily through the abdominal cavity after establishing the OA model. In total, 100 mg/kg of normal saline was given to both the sham and the ACLT groups through intraperitoneal injection. After 8 weeks of treatment, the rats were euthanized, and histological processing and analysis were conducted.

To further investigate, we attempted to block  $\beta$ OHB signaling using mepenzolate bromide (HCAR2 inhibitor), Compound C (AMPK antagonist), and mitochondrial division inhibitor-1 (Mdivi-1, mitochondrial division inhibitor). In the third round of animal experiments, 30 rats were randomized into 6 groups: sham group, ACLT group, ACLT + 200 mg/kg  $\beta$ OHB group, ACLT + 200 mg/kg  $\beta$ OHB + 10 mg/kg mepenzolate bromide group, ACLT + 200 mg/kg  $\beta$ OHB + 10 mg/kg Compound C group, and ACLT + 200 mg/kg  $\beta$ OHB + 2.5 mg/kg Mdivi-1 group. In a manner consistent with the protocol employed in the second round of the animal experiments, a daily administration of 200 mg/kg of  $\beta$ OHB was administered to the  $\beta$ OHB-supplemented group, while the group not receiving  $\beta$ OHB supplementation was injected with 200 mg/kg of normal saline. Administering 10 mg/kg of mepenzolate bromide via intraperitoneal injection reversed the protective effects of  $\beta$ OHB in an acute kidney injury model (Tran et al., 2016). Additionally, tail vein injection of 10 mg/kg Compound C inhibited the activity of AMPK (Yu et al., 2008). Mdivi-1 is a selective inhibitor of mitochondrial dynamin-related protein 1, which is widely used to hinder mitophagy (Liu et al., 2023). It has been demonstrated that 2.5 mg/kg Mdivi-1 could effectively impede mitophagy without notable impact on cellular function (Hinge et al., 2020). Consequently, 10 mg/kg mepenzolate bromide (HY-17585, MedChemExpress), 10 mg/kg Compound C (HY-13418, MedChemExpress) or 2.5 mg/kg Mdivi-1 (HY-15886, MedChemExpress) was administered via intra-articular administration an hour prior to  $\beta$ OHB treatment. Following an eight-week treatment period, the rats were euthanized, and subsequent histological processing and analysis were carried out.

## 2.17 | Histological assessment

Hematoxylin-eosin (H & E) and safranin O-fast green were used to stain paraffin sections. The assessment of pathological changes was conducted by two observers using the Osteoarthritis Research Society International (OARSI) through blinded graded observations (Pritzker et al., 2006). The H & E staining protocol includes deparaffinization of paraffin-embedded sections in xylene for a duration of 10 min, followed by hydration in a series of ethanol solutions. Subsequent steps involve incubation of the sections in hematoxylin staining solution for 5 min, followed by eosin staining for 1 min. Safranin O-fast green staining is achieved by immersing the sections in Fast Green FCF (0.02%) for 5 min and Safranin O (0.1%) for 1 min

TABLE 2 Basic nutrient content of the standard diet and ketogenic diet (per 100 g).

Component/item	Standard diet	Ketogenic diet
Energy (kJ)	1338.0	2804.0
Protein (g)	14.6	18.2
Fat (g)	4.0	65.2
Carbohydrates (g)	55.6	2.8
Dietary fibers (g)	4.6	7.4
Calcium (mg)	720.0	500.0
Phosphorus (mg)	600.0	300.0
Vitamin D ( $\mu\text{g}$ )	2.6	2.6

(Liu et al., 2022). The grading system employed included Grade 0 to indicate an intact surface and cartilage, Grade 1 for an intact surface only, Grade 2 for surface discontinuity, Grade 3 for vertical fissures, Grade 4 for erosion, Grade 5 for denudation, and Grade 6 for deformation. In the context of immunohistochemistry experiments, antigen retrieval is carried out after dewaxing and rehydration by subjecting the sections to 10 mmol/L citrate buffer at 100°C for a duration of 30 min. The endogenous peroxidase activity and non-specific antigen in the samples were blocked using a 3% hydrogen peroxide solution and serum (Du et al., 2020). Paraffin sections were subjected to incubation with primary antibodies targeting IL6 (1:50, TD6087, Abmart), Col2a1 (1:100, GB11021, Servicebio), MMP13 (1:100, 18165-1, Proteintech), P16 (1:200, ab54210, Abcam), P21 (1:50, PA9426, Abmart), PINK1 (1:50, TD7742, Abmart), p-Parkin (1:200, PA5-114616, Thermo Fisher); Parkin (1:50, A0968, Abclonal), P62 (1:50, TA5384, Abmart), HCAR2 (1:50, A15611, Abclonal), BAX (1:1000, 50599-2, Proteintech), and p-AMPK (1:100, 2535, Cell Signaling Tech). Subsequently, the sections were treated with goat anti-rabbit secondary antibody (1:100, G-21234, Thermo Fisher Scientific), developed using 3,3-diaminobenzidine solution, and counterstained with hematoxylin. Representative fields of view were captured with a light microscope. The immunohistochemistry images were quantified and analyzed using the ImageJ software (version 1.8).

## 2.18 | Statistical analysis

The data were analyzed using SPSS 22.0 software and plotted using GraphPad Prism 8.0.2 software. The results were presented as mean  $\pm$  standard deviation. For continuous variables, an unpaired Student's t-test was used to compare two groups, while a one-way ANOVA was used to compare multiple groups. For datasets with two parameters, two-way ANOVA was applied. The nonparametric data (OARSI scores) were analyzed using the Kruskal-Wallis H test. Statistical significance was defined as  $p < 0.05$ .

## 3 | RESULTS

### 3.1 | KD attenuated OA progression in a rat model

An OA model was built by ACLT to investigate the effects of KD on OA disease progression (Figure 1a). Neither KD nor ACLT exhibited a significant effect on the body weight of rats at any time point (Figure 1b). In the knee synovial fluid of rats subjected to the SD diet, a statistically significant decrease in  $\beta$ OHB concentration was observed compared to the sham-operated group at weeks 6–8 post-ACLT modeling (Figure 1c,  $p < 0.05$ ). KD treatment resulted in a significant increase in  $\beta$ OHB concentration in both serum and synovial fluid (Figure 1c, d,  $p < 0.05$ ). Furthermore, ACLT led to a significant increase in nitric oxide, TNF- $\alpha$ , IL6, and PGE2 levels in the serum, whereas KD reversed these alterations (Figure 1e–h,  $p < 0.05$ ). H &

E staining and safranin O-fast green staining revealed erosion and even cracking of the articular cartilage surfaces, loss of proteoglycan staining, and elevated OARSI scores in the ACLT + SD group (Figure 1i–k). However, the administration of KD resulted in the reversal of these pathological changes (Figure 1j, k). These findings indicate that KD has the potential to slow down OA progression in rats, and this effect may be attributed to the elevation of  $\beta$ OHB concentration in synovial fluid.

### 3.2 | Effect of $\beta$ OHB on chondrocyte viability

As a derivative of hydrogen peroxide, TBHP is extensively used in the modeling of osteoarthritic chondrocytes and has been shown to significantly induce oxidative stress, senescence, apoptosis, and extracellular matrix degradation in chondrocytes (He et al., 2024; Lu et al., 2021; Lv et al., 2022). To determine the optimal intervention concentration, the impact of  $\beta$ OHB or TBHP on chondrocyte viability was evaluated using the CCK-8 assay at various concentrations and time points. It was observed that  $\beta$ OHB exhibited no significant cytotoxicity within the concentration range of 0.5–8 mM, whereas TBHP significantly decreased chondrocyte viability at concentrations exceeding 5  $\mu$ M (Figure S1a, b,  $p < 0.05$ ). Furthermore, the ratio of SA- $\beta$ -Gal positive cells increased following TBHP intervention (Figure S1c, d,  $p < 0.01$ ), and the mRNA expression levels of P16 and P21 exhibited a significant increase in a concentration-dependent manner (Figure S1e,  $p < 0.05$ ). OA is a chronic degenerative disease characterized by persistent oxidative stress. To replicate this oxidative stress in vitro, we treated chondrocytes with TBHP at a relatively mild concentration of 15  $\mu$ M. CCK-8 assay results demonstrated that  $\beta$ OHB effectively mitigated the cytotoxic effects of TBHP, particularly within the concentration range of 1–4 mM (Figure S1f,  $p < 0.05$ ). Given the observed HCAR2 agonist activity of  $\beta$ OHB at a potency of 0.9 mM (Mao et al., 2023), we selected 1 or 4 mM of  $\beta$ OHB and 15  $\mu$ M of TBHP for subsequent chondrocytes interventions.

### 3.3 | $\beta$ OHB attenuates TBHP-induced SASP in chondrocytes

We next investigated the effects of  $\beta$ OHB on TBHP-induced chondrocyte senescence. SA- $\beta$ -Gal staining revealed that  $\beta$ OHB effectively decreased the incidence of senescent chondrocytes in TBHP-induced cells (Figure S2a, b,  $p < 0.01$ ). Alcian blue staining was utilized to assess the distribution and content of glycosaminoglycans produced by cells, with a positive correlation observed between the depth of staining and the secretion of Aggrecan by chondrocytes (Yu et al., 2021). The treatment with TBHP significantly suppressed Aggrecan secretion, while the treatment with  $\beta$ OHB partially relieved the adverse effects of TBHP (Figure S2c, d,  $p < 0.05$ ). Immunofluorescence staining demonstrated a decreased expression of anabolic biomarkers, including Aggrecan and Col2a1 expression, in the TBHP group compared to the control group



(Figure S2e–g,  $p < 0.01$ ). Surprisingly, the fluorescence intensity of Aggrecan and Col2a1 was restored by the treatment with  $\beta$ OHb (Figure S2e–g,  $p < 0.01$ ). Furthermore, RT-qPCR analysis revealed that TBHP intervention led to an upregulation of P16, P21, IL6, and

MMP13 expression, while Aggrecan and Col2a1 expression were down-regulated (Figure S2h–j,  $p < 0.05$ ). The western blotting results demonstrated a significant upregulation in the protein expression of iNOS, P16, P21, IL6, and MMP13 in the TBHP group, indicating that

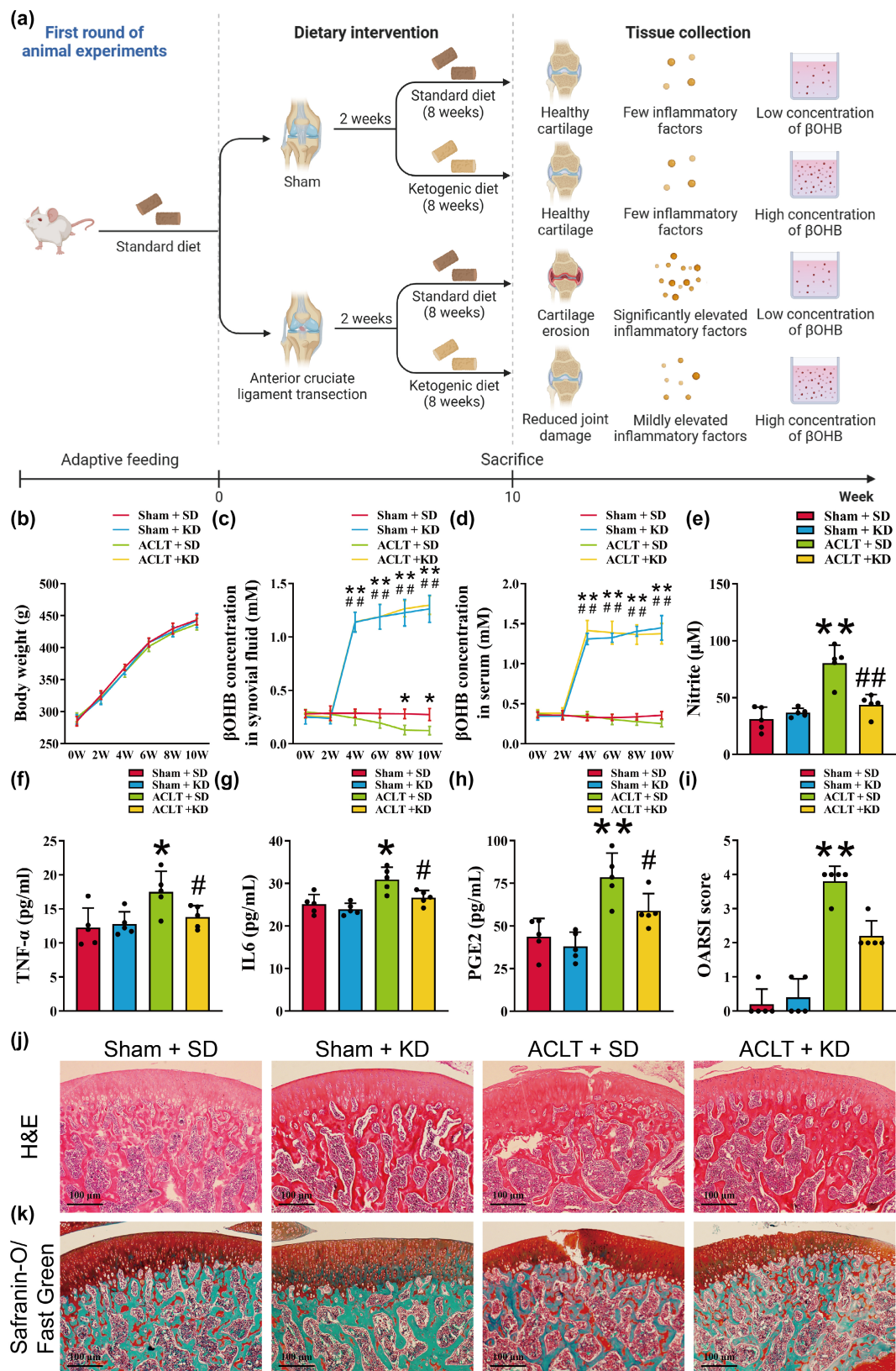


**FIGURE 1** Ketogenic diet (KD) attenuated osteoarthritis (OA) progression in a rat model. (a) The schematic diagram of animal experiments. (b) The body weight of the rats was measured at various time points. (c) The  $\beta$ OHB levels in the synovial fluid were measured at different time points. (d) The serum  $\beta$ OHB levels were assessed at different time points. (e) The concentration of nitric oxide was quantified using Griess reagent. (f-h) The concentrations of interleukin-6 (IL-6), tumor necrosis factor- $\alpha$  (TNF- $\alpha$ ), and prostaglandin E2 (PGE2) in the rat serum were determined through enzyme-linked immuno sorbent assay. (i) The OARSI scores of knee cartilage were recorded. (J) Representative images of hematoxylin-eosin (H & E) staining were captured, with a scale bar of 100  $\mu$ m. (k) Representative images of safranin O-fast green staining were obtained, with a scale bar of 100  $\mu$ m.  $n=5$ . Data in (b-d) were analyzed by the two-way ANOVA, data in (e-h) were analyzed by the one-way ANOVA, and data in (i) were analyzed by the Kruskal-Wallis H test. \* $p<0.05$ , \*\* $p<0.01$  versus the sham + SD group; # $p<0.05$ , ## $p<0.01$  versus the ACLT + SD group.

the intervention of 15  $\mu$ M TBHP induced the emergence of chondrocyte SASP phenotype (Figure S2k, l,  $p<0.05$ ). Besides, RT-qPCR and western blotting results indicated that the intervention of  $\beta$ OHB partially mitigated the impact of TBHP on SASP-related molecules (P16, P21, IL6, MMP13, iNOS, Aggrecan, and Col2a1) (Figure S2h-l,  $p<0.05$ ). The above findings provide evidence suggesting that  $\beta$ OHB exerts a beneficial effect on the SASP induced by TBHP in chondrocytes.

### 3.4 | $\beta$ OHB reduces TBHP-induced oxidative stress and chondrocyte apoptosis

It is well-established that the accumulation of ROS plays a crucial role in chondrocyte senescence (Chen et al., 2023). Therefore, we further investigated the impact of  $\beta$ OHB on TBHP-induced oxidative stress and apoptosis. Our results demonstrated that TBHP significantly increased the fluorescence intensity of ROS in both chondrocytes and mitochondria, whereas treatment with  $\beta$ OHB significantly reduced the intracellular accumulation of ROS in chondrocytes (Figure 2a-c). Furthermore, the flow cytometry analysis revealed that  $\beta$ OHB mitigated the increase in intracellular RNS induced by TBHP (Figure 2d).

Given that excessive oxidative stress has been linked to DNA damage and apoptosis (Arra et al., 2022), we investigated the impact of  $\beta$ OHB on apoptosis. The comet assay results demonstrated that TBHP led to observable tailing in cells, indicative of cellular DNA damage, whereas treatment with  $\beta$ OHB resulted in a reduction in comet tail length relative to the entire cell (Figure 2e, f,  $p<0.01$ ). The flow cytometry results demonstrated an increase in the apoptosis ratio of chondrocytes following TBHP intervention, which was subsequently reduced by  $\beta$ OHB treatment (Figure 2g, h,  $p<0.05$ ). Caspase-3 is a widely expressed member of a conserved family of proteins, generally recognized for their activated proteolytic roles in the execution of apoptosis (Eskandari & Eaves, 2022). Our research also indicated that TBHP exposure heightened caspase-3 activity in cells, whereas  $\beta$ OHB treatment led to a decrease in caspase-3 activity (Figure 2i,  $p<0.01$ ). Moreover, the results obtained from RT-qPCR and western blotting analyses demonstrated that TBHP caused a decrease in the mRNA and protein levels of CAT, SOD1, and BCL2, while simultaneously increasing the expression of cleaved Caspase-3, cleaved PARP-1, and BAX (Figure 2j-p,  $p<0.05$ ). Conversely,  $\beta$ OHB treatment reversed these alterations

(Figure 2j-p,  $p<0.05$ ). These findings suggest that  $\beta$ OHB possesses a protective effect against TBHP-induced oxidative stress and chondrocyte apoptosis.

### 3.5 | $\beta$ OHB improves mitophagy in TBHP-induced chondrocytes

The accumulation of dysfunctional mitochondria in senescent chondrocytes has been identified as the cause of increased levels of ROS within the cells. It has been observed that restoring mitochondrial function can effectively inhibit chondrocyte senescence (Shang et al., 2023). The measurement of  $\Delta\psi_m$  serves as a sensitive indicator of mitochondrial function, and the fluorescent probe JC-1 is commonly used to detect  $\Delta\psi_m$ . Under normal physiological conditions, JC-1 primarily exists in a polymer form, emitting red fluorescence. However, during the early stages of apoptosis, the reduction in  $\Delta\psi_m$  causes JC-1 to transition to a monomeric form, emitting green fluorescence. Consequently, a decrease in the red/green fluorescence ratio indicates mitochondrial depolarization and loss of membrane potential due to damage (Tao et al., 2024). In comparison to the control group, chondrocytes in the TBHP group exhibited a significant reduction in red light intensity and an increase in green light intensity, indicating a decrease in  $\Delta\psi_m$ . Conversely, intervention with  $\beta$ OHB partially reversed the decrease in  $\Delta\psi_m$  induced by TBHP (Figure 3a, b,  $p<0.05$ ).

Mitophagy, a process that selectively eliminates damaged or dysfunctional mitochondria through autophagic machinery, plays a crucial role in maintaining mitochondrial quality control and homeostasis (Sun et al., 2021). Our hypothesis posits that mitochondrial autophagy serves as a critical mechanism by which  $\beta$ OHB preserves mitochondrial membrane potential. The results of the immunofluorescence analysis indicated that TBHP induced upregulation of the intracellular mitochondrial autophagy markers LC3B and PINK1, while downregulating the expression of the outer mitochondrial membrane receptor TOMM20 (Figure 3c-f). TOMM20 is a protein located in the outer membrane of mitochondria, serving as a marker for mitochondrial quality (Konig et al., 2021). Analysis of TOMM20 morphology indicated that healthy cell mitochondria exhibited a consistent tubular form, whereas exposure to TBHP resulted in heightened mitochondrial fragmentation (Figure 3g). Furthermore, treatment with  $\beta$ OHB led to further enhancement of LC3B and PINK1 expression, as well as facilitated co-localization of



LC3B, PINK1 and TOMM20, indicating promotion of mitophagy by  $\beta$ OHB (Figure 3c–e, h). Analysis using transmission electron microscopy revealed damaged mitochondria with low cristae abundance following TBHP intervention, while treatment with  $\beta$ OHB resulted in improved mitochondrial structure and enhanced formation of

autophagolysosomes with mitochondrial-like organelles (Figure 3i). Our findings demonstrated that TBHP induced an upregulation in the proportion of damaged mitochondria characterized with low cristae abundance. Conversely, treatment with  $\beta$ OHB resulted in an increased proportion of mitochondria exhibiting high cristae

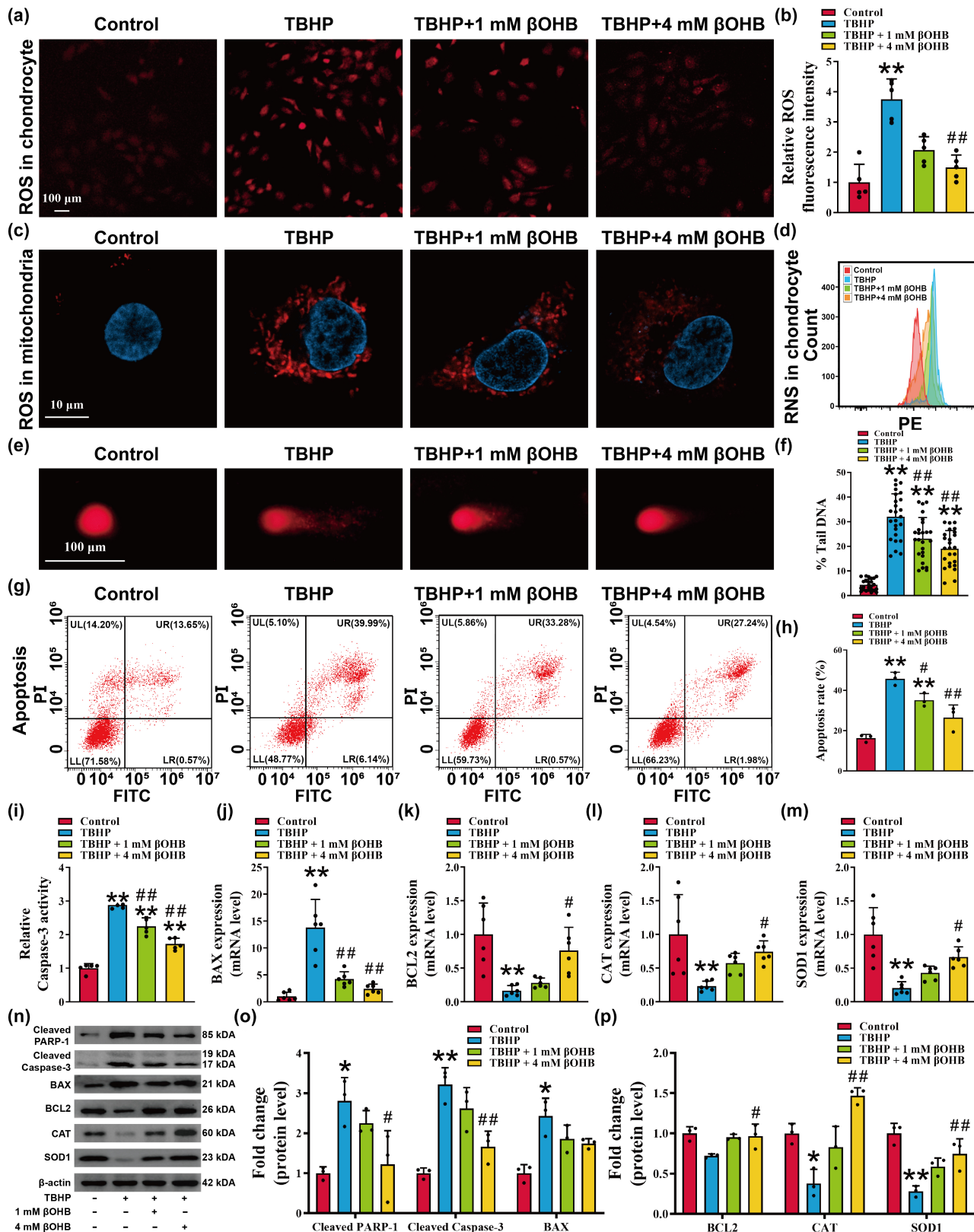




**FIGURE 2**  $\beta$ OHB reduces TBHP-induced oxidative stress and chondrocyte apoptosis. (a, b) ROS levels in chondrocytes were measured, with a scale bar of  $100\mu\text{m}$ ,  $n=5$ . (c) Representative images of mitochondria ROS were obtained through confocal microscopy, with a scale bar of  $10\mu\text{m}$ . (d) The reactive nitrogen species of chondrocytes was assessed using flow cytometry. (e) Representative images of the comet experiment were captured, with a scale bar of  $100\mu\text{m}$ . (f) Quantification of the tail DNA content (tail DNA intensity/cell DNA intensity) of the comet experiment,  $n=25$ . (g, h) The apoptosis ratio of chondrocytes was assessed using flow cytometry,  $n=3$ . (i) Caspase-3 activity in total cell lysates was measured using the Caspase-3 substrate, acetyl-Asp-Glu-Val-Asp. The activity was normalized to total protein concentration and presented as fold activity to the control group. (j-m) The mRNA expression levels of BAX, BCL2, CAT, and SOD1 were quantified using reverse transcription-quantitative polymerase chain reaction (RT-qPCR),  $n=6$ . (n-p) The protein expression levels of cleaved PARP-1, cleaved Caspase-3, BAX, BCL2, CAT, and SOD1 were analyzed using western blotting,  $n=3$ . The obtained data were subjected to analysis using the one-way ANOVA statistical method.  $^*p<0.05$ ,  $^{**}p<0.01$  versus the control group;  $^{\#}p<0.05$ ,  $^{##}p<0.01$  versus the TBHP group.

abundance, an elevated cristae density-to-perimeter ratio, and an enhanced frequency of mitophagy events, while concurrently reducing the percentage of damaged mitochondria (Figure 3j-m).

Activation of PINK1/Parkin activation through phosphorylation of its ubiquitin and ubiquitin-like domain by PINK1 plays a crucial role in inducing mitophagy (Niu et al., 2020). The western blotting analysis revealed that the control group exhibited low levels of mitophagy, as evidenced by the low expression of PINK1, p-Parkin, Parkin, P62, LC3B II, and p-Ub (Figure 4a-c). However, the intervention of TBHP slightly augmented the expression of PINK1, p-Parkin, Parkin, LC3B II, and p-Ub, indicating the initiation of mitophagy (Figure 4a-c,  $p>0.05$ ). Nevertheless, the accumulation of P62 indicated a disruption in autophagic flux within the TBHP group (Figure 4a, c,  $p<0.05$ ). Conversely, the administration of  $\beta$ OHB not only further enhanced the expression of PINK1, p-Parkin, Parkin, LC3B II, and p-Ub but also reduced the expression of P62, thereby indicating the restoration of cellular autophagy (Figure 4a-c,  $p<0.05$ ). Next, we investigated the impact of inhibiting mitophagy with Mdivi-1 on apoptosis. Previous research demonstrated that  $50\mu\text{M}$  Mdivi-1 effectively suppressed the expression of PINK1 and Parkin in chondrocytes (Liu et al., 2023). Therefore, we utilized the same concentration for our intervention. Flow cytometry analysis revealed a significant increase in apoptosis in chondrocytes following TBHP treatment. Interestingly, the addition of Mdivi-1 prevented  $\beta$ OHB from reversing the detrimental effects of TBHP (Figure 4d,  $p<0.05$ ). These findings indicate that  $\beta$ OHB has the potential to mitigate chondrocyte apoptosis induced by TBHP through the promotion of mitophagy.

### 3.6 | Supplementation of $\beta$ OHB alleviated OA progression in rats

To further assess the impact of  $\beta$ OHB in vivo, an experimental model of rat OA was established through ACLT (Figure S3a). The intragastric administration of  $\beta$ OHB did not result in a significant change in body weight in rats (Figure S3b). However, it did lead to a significant increase in  $\beta$ OHB concentrations in both synovial fluid and serum (Figure S3c, d). Additionally,  $\beta$ OHB alleviated the levels of nitric oxide, TNF- $\alpha$ , IL6, and PGE2 in the serum of OA rats (Figure S3e-h). Histological examination utilizing H & E and safranin O-fast green staining revealed that  $\beta$ OHB at doses of 100

or 200 mg/kg mitigated cartilage degradation and lowered OARSI scores (Figure S3i-k). These findings indicate that the intraperitoneal administration of  $\beta$ OHB effectively attenuated the progression in OA rats.

Immunohistochemistry results further demonstrated that  $\beta$ OHB promoted HCAR2, Col2a1, PINK1, Parkin expression, decreased IL6, MMP13, P16, P21, and P62 expression in chondrocytes (Figure S4). Hence, the aforementioned significant findings suggest that the activation of mitophagy by  $\beta$ OHB may serve as a potential therapeutic approach for alleviating OA.

### 3.7 | $\beta$ OHB exerts chondroprotective effects via HCAR2

As a high-affinity receptor for  $\beta$ OHB, HCAR2 has been scientifically established to play a crucial role in maintaining normal  $\Delta\text{ym}$  in M2 macrophages (Chen et al., 2018). Therefore, we employed siRNA to suppress the expression of HCAR2 in chondrocytes and investigated whether the chondroprotective efficacy of  $\beta$ OHB relied on HCAR2 (Figure 5a, b,  $p<0.01$ ).

Flow cytometry results demonstrated that  $\beta$ OHB mitigated the accumulation of RNS in chondrocytes. Besides,  $\beta$ OHB reduced the accumulation of ROS in chondrocytes and mitochondria (Figure 5c-f). Immunofluorescence staining results showed that  $\beta$ OHB restored the expression of Col2a1 and Aggrecan in TBHP-treated chondrocytes (Figure 5g-i,  $p<0.01$ ). However, this phenomenon was not observed in chondrocytes with HCAR2 knockdown. In addition, Alcian blue staining demonstrated that the administration of  $\beta$ OHB did not mitigate the detrimental consequences of TBHP after the suppression of HCAR2 (Figure 5j, k,  $p<0.01$ ). The above results showed that  $\beta$ OHB was unable to reverse the phenotypic loss of chondrocytes caused by TBHP intervention in HCAR2 knockdown chondrocytes.

The SA- $\beta$ -Gal staining demonstrated that  $\beta$ OHB reversed the cellular senescence induced by TBHP in chondrocytes, but this effect was abolished following HCAR2 knockdown (Figure 5l, m,  $p<0.01$ ). Flow cytometry results indicated a significant reduction in the apoptosis ratio of chondrocytes following treatment with  $\beta$ OHB, but the knockdown of HCAR2 resulted in an increased apoptosis ratio (Figure 5n, o,  $p<0.05$ ). The comet assay demonstrated that in HCAR2 knockdown chondrocytes,  $\beta$ OHB was unable to mitigate



TBHP-induced DNA damage (Figure 5p, q,  $p < 0.05$ ). The above findings indicate that  $\beta$ OHB is ineffective in mitigating TBHP-induced chondrocyte oxidative stress damage and apoptosis after HCAR2 knockdown.

JC-1 results indicated that  $\beta$ OHB augmented the ratio of red fluorescence to green fluorescence, implying a reduction in the number of cells undergoing early apoptosis, while this effect of  $\beta$ OHB was nullified upon the inhibition of HCAR2 (Figure S5a, b,  $p < 0.01$ ).

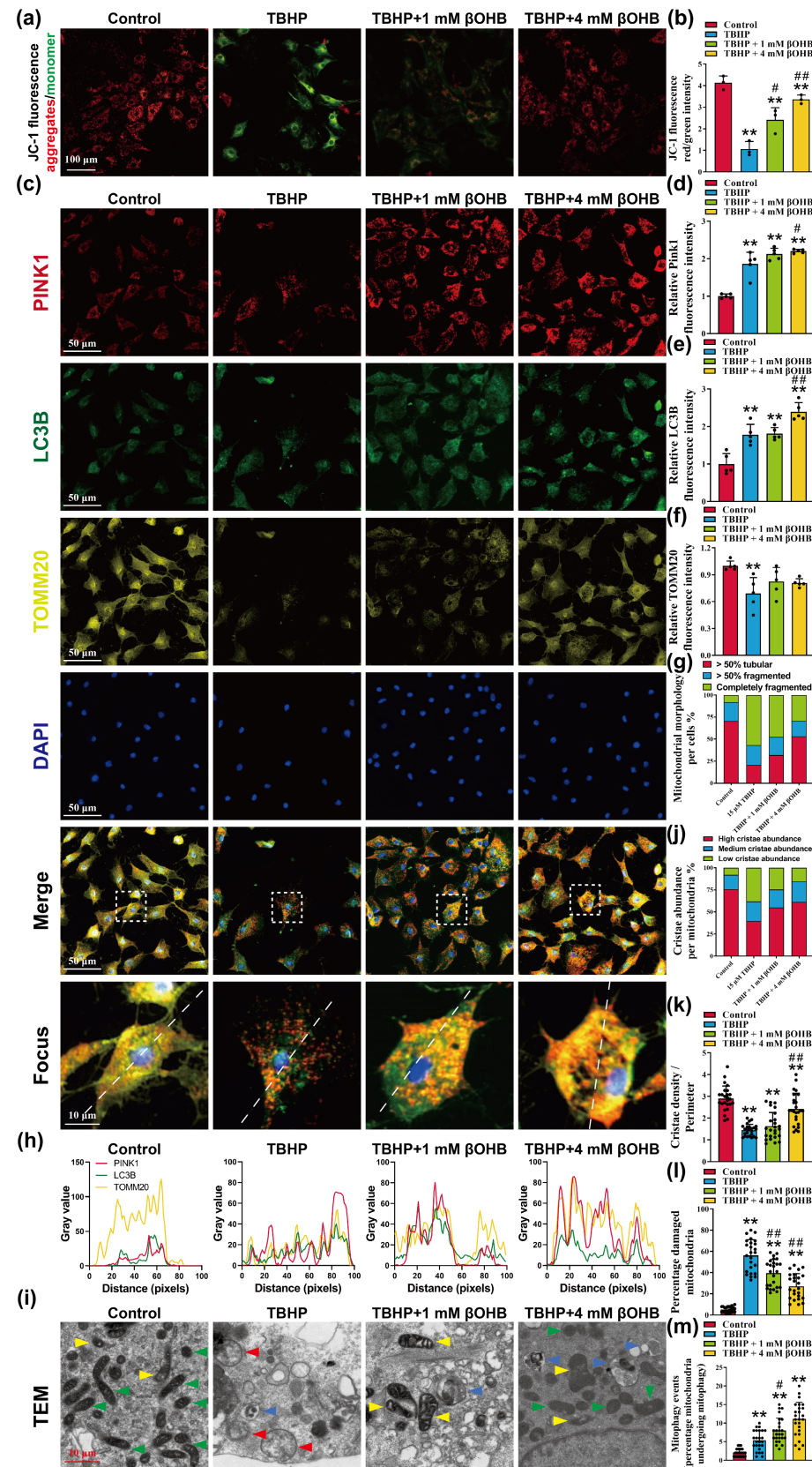


**FIGURE 3**  $\beta$ OHB improves mitophagy in TBHP-induced chondrocytes. (a, b) Representative images of mitochondrial membrane potential assay were obtained using JC-1, with a scale bar of 100  $\mu$ m,  $n=3$ . (c-f) Representative images and relative fluorescence intensity of PINK1 (red), LC3B (green), TOMM20 (yellow), and cell nuclei (blue) immunofluorescence were captured, with a scale bar of 50  $\mu$ m,  $n=5$ . (g) The ratio of tubular mitochondria and fragmented mitochondrial was observed based on the immunofluorescence staining results of TOMM20,  $n=25$ . (h) Co-localization of PINK1 (red), LC3B (green), TOMM20 (yellow). (i) Microstructural detection of mitophagy by transmission electron microscopy and normal mitochondria with high cristae abundance (green arrow), mitochondria with medium cristae abundance (yellow arrow), damaged mitochondria with low cristae abundance (red arrow), and autophagosomes with mitochondrial-like organelles (blue arrow) were as indicated, scale bar = 10  $\mu$ m. (j) The cristae abundance in mitochondria was quantified by the images of transmission electron microscopy,  $n=25$ . (k) The ratio of cristae density and perimeter in mitochondria was quantified by the images of transmission electron microscopy,  $n=25$ . (l, m) The percentage of damaged mitochondria and mitophagy events were quantified by the images of transmission electron microscopy,  $n=25$ . The obtained data were subjected to analysis using the one-way ANOVA statistical method. \* $p<0.05$ , \*\* $p<0.01$  versus the control group; # $p<0.05$ , ## $p<0.01$  versus the TBHP group.

Immunofluorescence analysis revealed that HCAR2 knockdown resulted in decreased LC3B and PINK1 expression, enhanced mitochondrial fragmentation, and hindered co-localization of LC3B, PINK1, and TOMM20 (Figure S5c-h). Transmission electron microscopy findings indicated that  $\beta$ OHB did not restore mitochondrial cristae abundance in HCAR2 knockdown chondrocytes, leading to an increase in damaged mitochondria and a reduction in mitochondrial autophagy events (Figure S5i-m).

RT-qPCR results revealed that  $\beta$ OHB downregulated the RNA expression of P16, P21, IL6, MMP13, and BAX, while upregulating the expression of Col2a1, Aggrecan, BCL2, CAT, and SOD1 in TBHP-stimulated chondrocytes, but the effects of  $\beta$ OHB diminished in chondrocytes with HCAR2 knockdown (Figure S6a, b,  $p<0.05$ ). The western blotting results revealed that  $\beta$ OHB significantly upregulated the expression of P16, P21, iNOS, IL6, MMP13, Cleaved PARP-1, Cleaved Caspase-3, BAX, PINK1, p-Parkin, Parkin, and LC3B II, and promoted the phosphorylation of ubiquitin, while downregulating the expression of BCL2, CAT, SOD1, and P62. Knockdown of HCAR2 resulted in suppressed expression of PINK1, Parkin, and LC3B II, and elevated expression of P62, indicating impaired mitophagy in chondrocytes (Figure S6c-e,  $p<0.05$ ). These results offer evidence for the beneficial effects of  $\beta$ OHB in mitigating TBHP-induced oxidative stress, apoptosis, and mitophagy in chondrocytes through the involvement of HCAR2.

### 3.8 | Effects of $\beta$ OHB on mitochondrial respiration and oxidative phosphorylation in chondrocytes

Mitochondria play a crucial role in meeting the energy demands of cells through the production of ATP. OA may arise when there is a disruption in energy metabolism leading to decreased ATP synthesis in chondrocytes (Chen et al., 2022).  $\beta$ OHB serves as a vital metabolic fuel that supports bioenergetic metabolism, particularly during periods of nutrient deprivation (Puchalska & Crawford, 2021). In tissues outside of the liver,  $\beta$ OHB is converted to acetyl-CoA and enters the tricarboxylic acid cycle through a series of enzymatic reactions known as ketolysis (Luda et al., 2023). Exposure of activated CD8 Teff cells to  $\beta$ OHB for a short duration (2 h) resulted in a modest increase in their basal OCR and ATP

production through oxidative phosphorylation (Luda et al., 2023). In order to assess the impact of  $\beta$ OHB on energy metabolism in chondrocytes, real-time evaluation of mitochondrial function was conducted using the Seahorse Bioscience XFp extracellular flux analyzer under different stimuli.

Basal respiration, maximal respiration, and spare respiratory capacity are intricately linked to cell viability (Dhingra & Kirshenbaum, 2015; Huang et al., 2019). Treatment with  $\beta$ OHB resulted in a slight increase in maximal respiration and spare respiratory capacity of chondrocytes in the absence of TBHP intervention compared to the control group (Figure S7a-d,  $p>0.05$ ). However, this difference did not reach statistical significance. TBHP intervention led to a decrease in basal respiration, maximal respiration, and spare respiratory capacity compared to the control group, indicating a reduction in ATP production capacity and severe mitochondrial dysfunction in chondrocytes (Figure S7a-d,  $p<0.05$ ). Meanwhile, a decrease in chondrocyte respiration was observed in response to the heightened oxidizing environment. Conversely, treatment with  $\beta$ OHB demonstrated the ability to mitigate mitochondrial oxidative damage by enhancing spare respiratory capacity, maximal respiration, and ATP production capacity, indicating its potential for mitigating such damage (Figure S7a-f,  $p<0.05$ ). Furthermore, a mild reduction in chondrocyte respiration was noted following HCAR2 knockdown, although this change did not reach statistical significance (Figure S7a-f,  $p>0.05$ ). Nevertheless, the therapeutic efficacy of  $\beta$ OHB against TBHP-induced damage was negated upon HCAR2 knockdown (Figure S7a-f,  $p<0.05$ ). The above findings suggest that  $\beta$ OHB regulates chondrocyte energy metabolism in chondrocytes subjected to oxidative stress.

### 3.9 | $\beta$ OHB exerts chondroprotective effects through phosphorylation of AMPK

AMPK is a heterotrimeric complex consisting of one catalytic subunit  $\alpha$  and two regulatory subunits  $\beta$  and  $\gamma$ , and is closely associated with energy metabolism (Yao et al., 2023).  $\beta$ OHB has been shown to activate the HCAR2/AMPK axis, leading to prevention of hepatic steatosis and the regulation of neutrophil-mediated inflammation (Carretta et al., 2020; Lee et al., 2020). Activation of AMPK can modulate cell metabolism through PINK1-PRKN-dependent mitophagy,

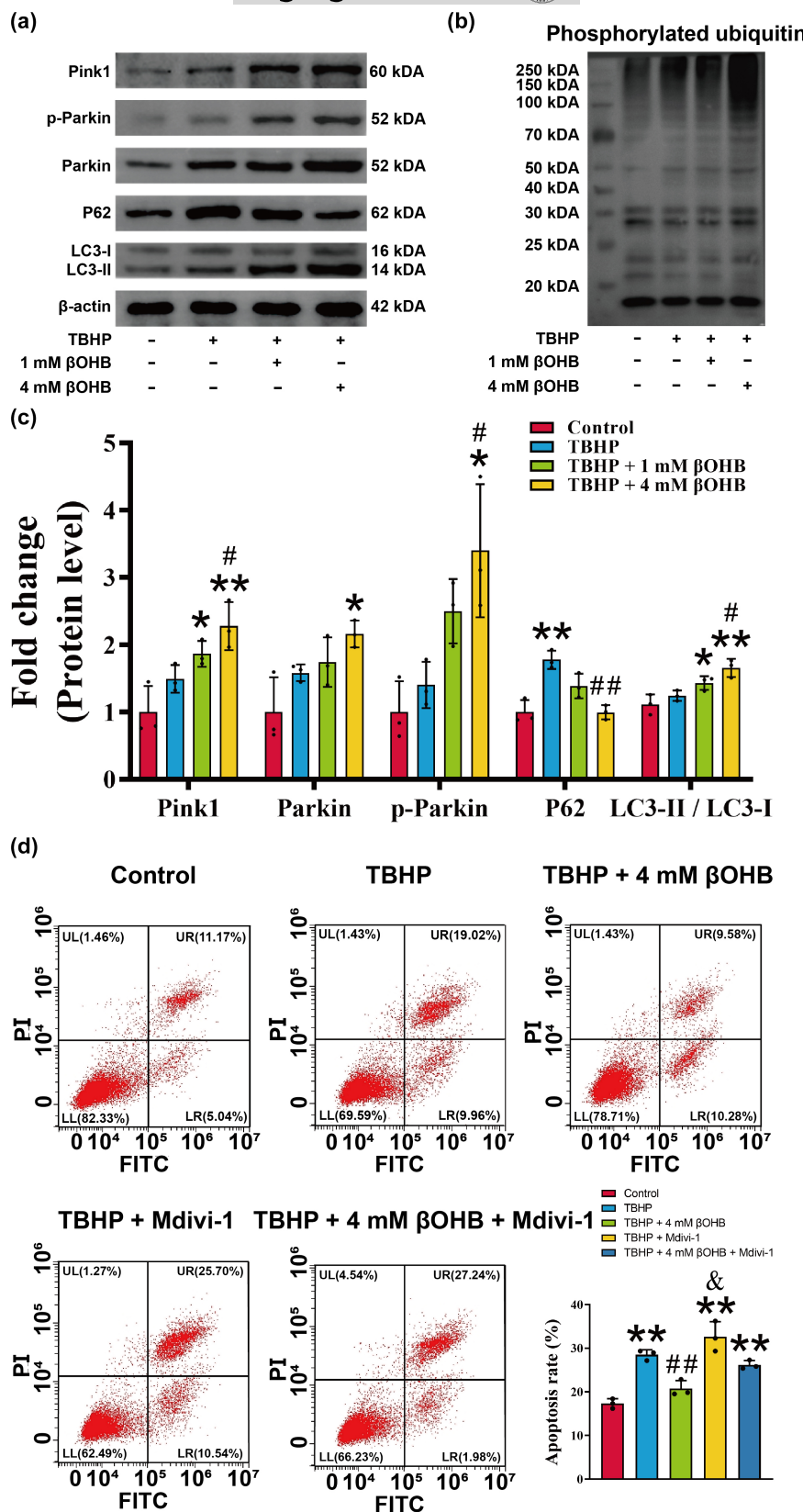


**FIGURE 4**  $\beta$ OHB improves mitophagy in TBHP-induced chondrocytes. (a) The protein expression levels of Pink1, p-Parkin, Parkin, P62, and LC3B were assessed using western blotting,  $n=3$ . (b) Phosphorylated ubiquitin was detected by western blotting. (c) The relative protein expression levels of Pink1, p-Parkin, Parkin, P62, and LC3B were quantified by the ImageJ software (version 1.8). (d) The apoptosis ratio of chondrocytes was assessed using flow cytometry,  $n=3$ . The obtained data were subjected to analysis using the one-way ANOVA statistical method.  $*p < 0.05$ ,  $**p < 0.01$  versus the control group;  $\#p < 0.05$ ,  $\#\#p < 0.01$  versus the TBHP group;  $\&p < 0.05$  versus the TBHP + 4 mM group  $\beta$ OHB group.

thereby improving renal oxidative stress and renal tubulointerstitial fibrosis in diabetic mice (Gong et al., 2022; Han et al., 2021). This suggests that  $\beta$ OHB may play a protective role in chondrocytes by targeting the HCAR2/AMPK/PINK1 axis.

The results of the western blot analysis indicated that intervention with TBHP led to a decrease in AMPK phosphorylation, while  $\beta$ OHB significantly increased AMPK phosphorylation in a manner dependent on HCAR2 (Figure 6a,  $p < 0.05$ ). Subsequently, the AMPK



antagonist Compound C (25  $\mu$ M) was utilized to further investigate the potential mechanisms. The western blot analysis revealed that inhibition of AMPK did not impact the upregulation of HCAR2 expression by  $\beta$ OHB intervention (Figure 6b, c). However, Compound C promoted SASP, oxidative stress and apoptotic phenotypes in chondrocytes (Figure 6b, c). Moreover, the expression of PINK1, Parkin, p-Parkin, and p-Ub was suppressed with Compound C, suggesting inhibition of mitophagy (Figure 6b-d). These findings suggest that  $\beta$ OHB exerts chondroprotective effects through the phosphorylation of AMPK.

### 3.10 | $\beta$ OHB exerts protective effects on OA rats through the HCAR2/AMPK/PINK1 pathway

To investigate the therapeutic mechanism of  $\beta$ OHB, mepenzolate bromide (HCAR2 inhibitor), Compound C (AMPK antagonist), and Mdivi-1 (mitochondrial division inhibitor) were injected into the knee joints of rats. H & E staining and safranin O-fast green staining results indicated that  $\beta$ OHB was unable to reverse the damage caused by ACLT after injection of the inhibitors (Figure S8a-c,  $p < 0.05$ ). Immunohistochemical staining showed that ACLT decreased the expression of HCAR2 and p-AMPK, while treatment with  $\beta$ OHB increased their expression (Figure S8d-i,  $p < 0.05$ ). Additionally, injection of mepenzolate bromide counteracted the pro-expression effects of  $\beta$ OHB on HCAR2, p-AMPK, PINK1, p-Parkin, and Parkin (Figure S8d-i,  $p < 0.05$ ). Compound C injection did not suppress HCAR2 expression but did inhibit p-AMPK levels and mitophagy (Figure S8d-i,  $p < 0.05$ ). In contrast, inhibition of mitophagy in rat cartilage tissue by Mdivi-1 injection did not alter the expression of HCAR2 and p-AMPK (Figure S8d-i,  $p < 0.05$ ). These findings support the conclusion that  $\beta$ OHB delays OA progression through the HCAR2/AMPK/PINK1 signaling pathway.

## 4 | DISCUSSION

OA is one of the predominant causes of disability in the elderly population. Regrettably, existing pharmaceutical interventions merely offer transient relief from OA pain symptoms, necessitating further exploration of drugs capable of impeding the pathogenesis of OA. TBHP, a well-established inducer of free radical reactions, is extensively employed in creating cellular models for oxidative stress and senescence (Jiang et al., 2022; Pan et al., 2023; Shang et al., 2023). While KD has demonstrated significant potential in suppressing inflammation and premature aging, it is important to acknowledge that KD may also elevate the likelihood of various disorders and diseases, such as kidney disease, fatigue, headache, and dizziness, thereby potentially impacting the health of patients, particularly the elderly who constitute the majority of the OA-affected population (Dynka et al., 2023; Ferrer et al., 2023; Gorini et al., 2023). Consequently, it becomes imperative to investigate alternative treatment strategies that are more viable.

Ketone bodies play a crucial role as an energy source in biological processes, with  $\beta$ OHB constituting approximately 70% of the overall circulating ketone bodies (Puchalska & Crawford, 2017). During periods of starvation, the concentration of  $\beta$ OHB in the bloodstream can rise to 8 mM, thereby becoming the primary source of energy for the body (Ji et al., 2022; Shimazu et al., 2013). Through synovial metabolomics analysis, it has been determined that  $\beta$ OHB serves as a significant biomarker for synovial inflammation in patients with OA (Mickiewicz et al., 2015). Recent findings have revealed that ketone bodies possess not only energy-carrying capabilities but also signaling functions (Newman & Verdin, 2014). This study demonstrated that both KD feeding and intraperitoneal injection of  $\beta$ OHB effectively mitigated disease progression in rats with OA. Additionally,  $\beta$ OHB exhibited the ability to reverse oxidative stress, apoptosis, and senescence induced by TBHP in chondrocytes, while maintaining the equilibrium between extracellular matrix synthesis and degradation. These findings suggest that  $\beta$ OHB shows promise as a potential therapeutic target for OA.

Chondrocytes, which exclusively constitute articular cartilage, play a crucial role in extracellular matrix synthesis by continuously secreting collagen type II and Aggrecan (Guilak et al., 2018). Type II collagen and Aggrecan are widely recognized as the predominant cartilage proteins and are commonly utilized as classical biomarkers for OA (Bay-Jensen et al., 2022). Type II collagen, the primary protein found in cartilage, functions as a fibrillar collagen that provides structural support to the extracellular matrix of cartilage (Eyre, 2002). Aggrecan serves as the principal glycoprotein within the extracellular matrix of articular cartilage (Heinegard & Saxne, 2011). Aggrecan functions as the predominant glycoprotein in the extracellular matrix of articular cartilage, binding to hyaluronic acid and link proteins to attract cations and osmotically obligated water into the extracellular matrix (Kiani et al., 2002). This process results in the formation of a hydrated gel that imparts compressive strength to the cartilage. The degradation of type II collagen and Aggrecan in articular cartilage by matrix metalloproteinases is recognized as a significant pathological characteristic of OA (Zhang et al., 2009). MMP-13 is also acknowledged as a marker of terminal chondrocyte differentiation (Inada et al., 2004). Our findings indicate that treatment with  $\beta$ OHB leads to the downregulation of MMP13 expression and the promotion of col2a1 and Aggrecan expression, suggesting that  $\beta$ OHB may contribute to the maintenance of a healthy chondrocyte phenotype rather than a hypertrophic one.

Oxidative stress, characterized by an imbalance between oxidative and antioxidant activities, is recognized as a significant factor in aging and disease, and is implicated in the pathophysiology of OA (Zhuang et al., 2018). To induce the production of ROS and RNS in cells, we utilized TBHP to induce the production of iNOS. iNOS serves as a pivotal enzyme in the synthesis of nitric oxide and the sustained activity of nitric oxide can lead to the inhibition of extracellular matrix secretion in chondrocytes (Ahmad et al., 2020). This disruption in extracellular matrix balance within the cartilage microenvironment ultimately results in the quality of cartilage deteriorates (Santoro et al., 2015). After experiencing injury, such as oxidative stress, chondrocytes can

maintain the balance of cartilage through adaptive cell proliferation. However, chondrocytes that re-enter the cell division cycle in this manner are more prone to cellular senescence, which contributes to the progression of OA (Coryell et al., 2021). Senescent chondrocytes

not only display a portion of chondrocytes that are positive for SA- $\beta$ -Gal and increased levels of P16 and P21, but also release inflammatory factors and enzymes that degrade the extracellular matrix (Tsuchida et al., 2014). The upregulation of SASP factors initiates an

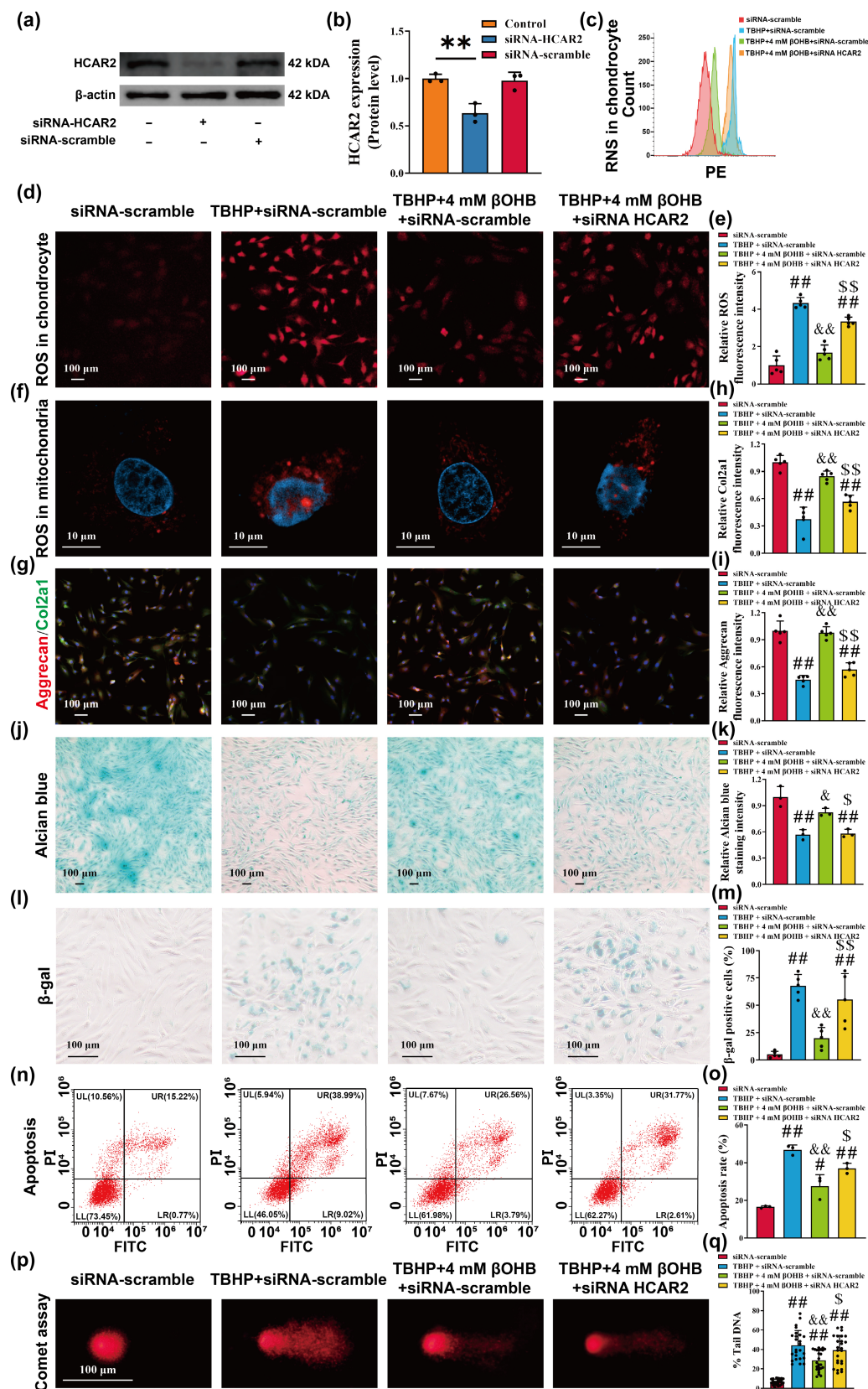




**FIGURE 5**  $\beta$ OHB exerts chondroprotective effects via HCAR2 in TBHP-induced chondrocytes. (a, b) The protein expression levels of HCAR2 were evaluated by western blotting,  $n=3$ . (c) The reactive nitrogen species of chondrocytes was assessed using flow cytometry. (d, e) ROS levels in chondrocytes were measured, with a scale bar of  $100\text{ }\mu\text{m}$ ,  $n=5$ . (f) Representative images of mitochondria ROS were obtained through confocal microscopy, with a scale bar of  $10\text{ }\mu\text{m}$ . (g–i) Representative images and relative fluorescence intensity of Aggrecan (red), Col2a1 (green), and cell nuclei (blue) immunofluorescence were captured, with a scale bar of  $100\text{ }\mu\text{m}$ ,  $n=5$ . (j, k) Representative images of Alcian Blue staining were obtained, with a scale bar of  $100\text{ }\mu\text{m}$ . (l, m) Senescence-associated  $\beta$ -galactosidase (SA- $\beta$ -gal) staining was utilized to observe the aging phenotype, with a scale bar of  $100\text{ }\mu\text{m}$ ,  $n=5$ . (n, o) The apoptosis ratio of chondrocytes was assessed using flow cytometry,  $n=3$ . (p) Representative images of the comet experiment were captured, with a scale bar of  $100\text{ }\mu\text{m}$ . (q) Quantification of the tail DNA content (tail DNA intensity/cell DNA intensity) of the comet experiment,  $n=25$ . The obtained data were subjected to analysis using the one-way ANOVA statistical method. \*\* $p<0.01$  versus the control group; # $p<0.05$ , ## $p<0.01$  versus the siRNA-scramble group; & $p<0.05$ , && $p<0.01$  versus the TBHP+siRNA-scramble group; \$ $p<0.05$ , \$\$ $p<0.01$  versus the TBHP+4 mM  $\beta$ OHB+siRNA-scramble group.

inflammatory response and senescence in neighboring healthy cells, ultimately resulting in extracellular matrix degradation and cartilage degeneration (Jeon et al., 2018). Mitigating chondrocyte senescence diminishes the production of MMPs and pro-inflammatory factors, thereby preserving the structural integrity of articular cartilage (Xie et al., 2021). Activation of the cell death program occurs when cellular stress surpasses a critical threshold in intensity or duration. Upon initiation of the apoptotic program, caspases are activated to cleave a diverse array of proteins in order to facilitate apoptosis. Caspase-3, a member of the Cysteine-ASPartic proteASES family renowned for their role in mediating the specific cleavage of substrates during apoptosis, is responsible for cleaving various downstream proteins, ultimately leading to the characteristic morphological changes observed in apoptotic cells (Eskandari & Eaves, 2022). Our findings indicate that the cleavage of PARP-1 by activated caspase-3 results in PARP-1 inactivation and subsequent inhibition of DNA repair capabilities, as evidenced by a notable increase in tail DNA percentage in the comet experiment.

Although  $\beta$ OHB has been reported to inhibit oxidative stress in various studies, its role in OA remains inadequately explored (Kawakami et al., 2022; Luo et al., 2022; Miyauchi et al., 2019). Our findings demonstrate that  $\beta$ OHB significantly attenuates the expression of senescence markers (p16, p21, SA- $\beta$ -Gal), inflammatory factors (IL6, iNOS), apoptotic markers (BAX, cleaved caspase-3, cleaved PARP-1), and promotes the synthesis of extracellular matrix (Aggrecan and Col2a1), thereby enhancing chondrocyte resilience against oxidative stress induced by TBHP.

The articular cartilage lacks blood vessels and instead receives nutrients and oxygen through the diffusion of synovial fluid and substances from the subchondral bone (Milner et al., 2006). The oxygen concentration at the surface of the joint is approximately 6%, while it decreases to 1% in the deeper layers of the cartilage, indicating a consistently low oxygen environment (Shimomura et al., 2022). Chondrocytes affected by OA frequently demonstrate the release of pro-inflammatory cytokines, damage from oxidative stress, impaired mitochondrial energy metabolism, and imbalances in protein metabolism, all of which significantly impact the physiological function of the cartilage tissue (Xu et al., 2020). While normal cartilage metabolism primarily occurs in the absence of oxygen, joints affected by OA commonly exhibit mitochondrial dysfunction (Blanco & Rego-Perez, 2020). Cellular autophagy is the process by which intracellular proteins and organelles are degraded by lysosomes.

Mitophagy, a specific form of cellular autophagy, is responsible for the removal of dysfunctional mitochondria and serves as a vital regulatory mechanism for maintaining cellular homeostasis. Mitophagy plays a pivotal role in preventing the generation of ROS and mitochondrial dysfunction, thereby aiding chondrocytes in their survival during pathological circumstances (Fernandez-Moreno et al., 2022). Mitophagy dysfunction is observed in various age-related ailments, and interventions aimed at enhancing mitophagy have exhibited encouraging outcomes in the context of muscle senescence, cardiovascular disorders, and neurological degenerative conditions (Palikaras et al., 2017). Consequently, the exploration of mitophagy targeting is deemed an efficacious strategy for addressing OA.

$\beta$ OHB has been identified as a high-affinity ligand for HCAR2, although the specific role of HCAR2 in chondrocytes remains unknown (Rahman et al., 2014). HCAR2 is a G protein-coupled receptor widely expressed on cell membranes. The activation of HCAR2 by  $\beta$ OHB and nicotinic acid, leading to anti-inflammatory effects, presents an intriguing potential for targeting this receptor in the treatment of gastrointestinal, cardiovascular, and neurogenic inflammatory disorders (Chen et al., 2018; Dmitrieva-Posocco et al., 2022; Kaye et al., 2020; Moutinho et al., 2022; Singh et al., 2014). To the best of our knowledge, there is a lack of research on the role of HCAR2 in chondrocytes. Despite the strong agonist activity of nicotinic acid as a small molecule carboxylic acid, the side effects of cutaneous flushing pose a challenge to patient compliance (Walters et al., 2009). Therefore, our study focuses on the potential role of  $\beta$ OHB and its receptor HCAR2 in OA. The unanticipated necessity of HCAR2 in the anti-oxidative stress properties of  $\beta$ OHB is noteworthy, considering that  $\beta$ OHB has previously demonstrated anti-inflammatory effects by directly inhibiting inflammasome activation, irrespective of its known activation of HCAR2 (Y. Chen et al., 2018). Our study found that  $\beta$ OHB failed to reverse the damaging effects of TBHP on HCAR2 knockdown chondrocytes, suggesting that the therapeutic effect of  $\beta$ OHB is dependent on HCAR2.

The PINK1/Parkin pathway is widely recognized as a significant mechanism of mitophagy (Onishi et al., 2021). In normal circumstances, PINK1 relocates to the inner mitochondrial membrane in a manner contingent upon membrane potential, followed by degradation to maintain minimal levels (Yamano & Youle, 2013). When the mitochondrial transmembrane potential is disrupted, PINK1 accumulates and facilitates the recruitment and activation of Parkin in the cytoplasm, thereby promoting mitophagy for the elimination

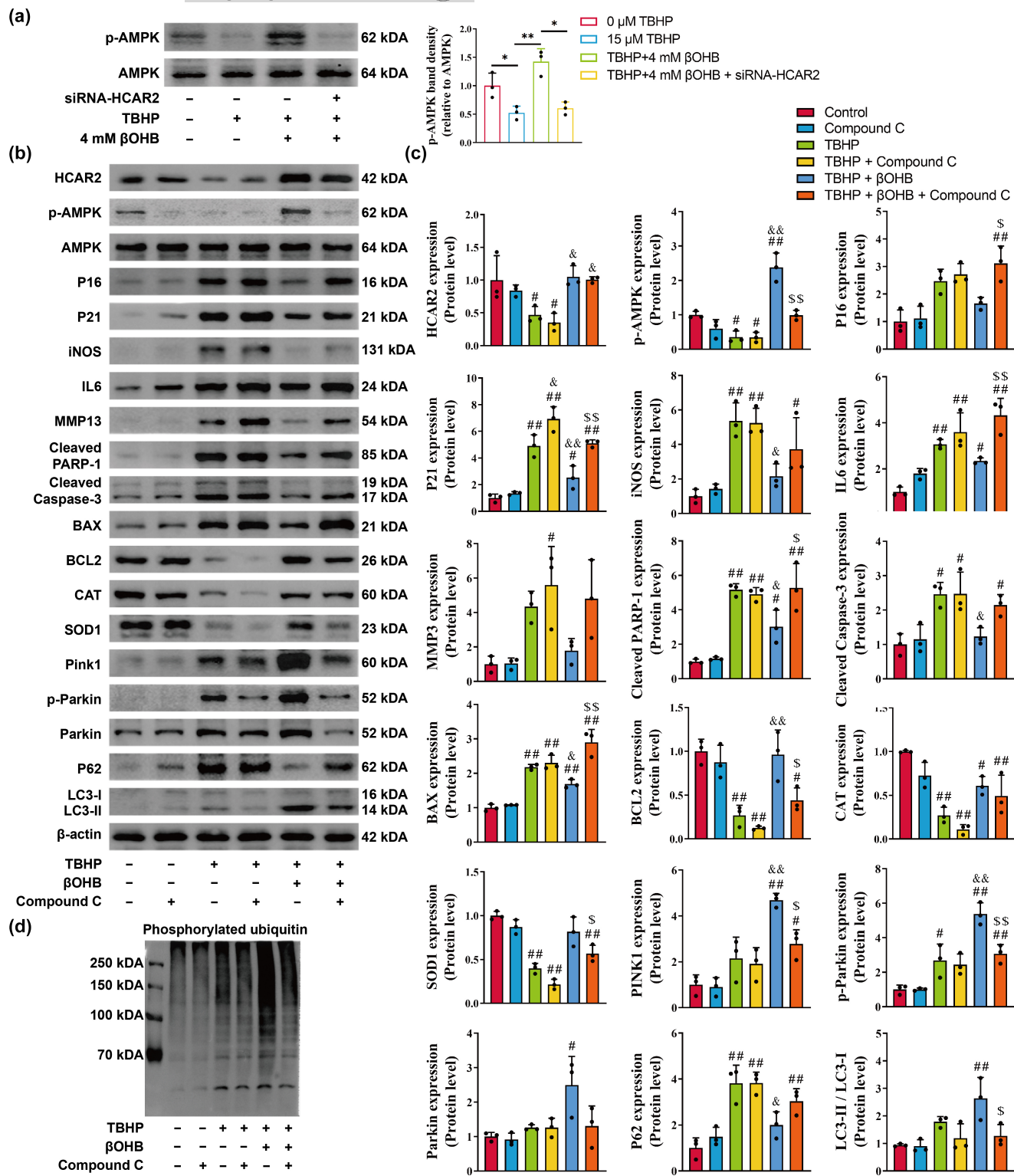


**FIGURE 6**  $\beta$ OHB exerts chondroprotective effects through activation of AMPK. (a) The protein expression level of p-AMPK was assessed using western blotting,  $n=3$ . (b) The protein expression levels of HCAR2, p-AMPK, AMPK, P16, P21, iNOS, IL6, MMP13, Cleaved PARP-1, Cleaved caspase-3, BAX, BCL2, CAT, SOD1, Pink1, p-Parkin, Parkin, P62, and LC3B were assessed using western blotting,  $n=3$ . (c) The relative protein expression levels of HCAR2, p-AMPK, AMPK, P16, P21, iNOS, IL6, MMP13, Cleaved PARP-1, Cleaved caspase-3, BAX, BCL2, CAT, SOD1, Pink1, p-Parkin, Parkin, P62, and LC3B were quantified by the ImageJ software (version 1.8). (d) Phosphorylated ubiquitin was detected by western blotting. The obtained data were subjected to analysis using the one-way ANOVA statistical method. \* $p < 0.05$ , \*\* $p < 0.01$ ; # $p < 0.05$ , ## $p < 0.01$  versus the Control group; & $p < 0.05$ , && $p < 0.01$ , versus the TBHP group; \$ $p < 0.05$ , \$\$ $p < 0.01$  versus the TBHP +  $\beta$ OHB group.



of impaired mitochondria (Geisler et al., 2010; Koyano et al., 2014). Parkin, an E3 ubiquitin ligase, exhibits robust expression in various tissues, implying a diverse array of physiological functions (Suen et al., 2010). The initiation of mitophagy through parkin recruitment is believed to entail the ubiquitylation of mitochondrial substrates by parkin, with its E3 ubiquitin ligase activity heightened upon translocation to mitochondria (Matsuda et al., 2010). Activation of PINK1-dependent mitophagy through the use of suberoylanilide hydroxamic acid results in a reduction of TOMM20, heat shock protein 60, and translocase of the inner membrane 23 protein levels (Sun et al., 2022). This process is also associated with an increase in LC3 protein levels (autophagosomal marker), and a decrease in P62 protein levels (autophagic substrate) (Sun et al., 2022). LC3 (also called MAP1LC3 or LC3B, the ortholog of yeast ATG8) undergoes synthesis in the pro-LC3 form, subsequent cleavage by ATG4B to generate LC3-I, and conjugation in ubiquitin-like reactions to phosphatidyl ethanolamine resulting in the formation of LC3-II. The localization of LC3-II to isolation membranes is essential for the elongation and closure of these membranes, ultimately leading to the formation of mature autophagosomes (Ashrafi & Schwarz, 2013). The accumulation of LC3-II is indicative of a late stage in the autophagy pathway and is dependent on various protein complexes crucial for mitophagy (Ashrafi & Schwarz, 2013). During the process of mitophagy, the accumulation of the ubiquitin-binding articulin protein P62 on depolarized mitochondria aids in the recruitment of damaged mitochondria to the autophagosome by binding to LC3 (Youle & Narendra, 2011). Conversely, the rapid accumulation of P62 following irreversible inflammation or oxidative stress implies the inhibition of mitophagy (Chen et al., 2020).

The involvement of mitophagy and associated proteins in OA remains a topic of debate (Sun et al., 2021). Chondrocytes stimulated with IL1 $\beta$  demonstrate characteristics of OA and an increase in mitophagy mediated by PRKN (Ansari et al., 2018). Depletion of PRKN results in impaired mitophagy, leading to mitochondrial dysfunction and oxidative stress (Ansari et al., 2018). Treatment with metformin activates the SIRT3-PINK1-PRKN signaling pathway, reversing IL1 $\beta$ -induced oxidative stress in chondrocytes (C. Wang et al., 2019). These findings underscore the significance of the PINK1-PRKN signaling pathway in regulating mitophagy and maintaining chondrocyte homeostasis in pathological conditions. In contrast, Shin et al. demonstrated that PINK1-mediated mitophagy led to mitochondrial fragmentation and cell death in human chondrocytes and rats following monosodium iodoacetate treatment (Shin et al., 2019). PINK1 knockout mice exhibited decreased cartilage damage and pain behavior in OA rats (Shin et al., 2019). These results indicate a dual impact of mitophagy on cellular survival and functionality, potentially influenced by varying levels of mitophagy in pathological states. Intriguingly, our study reveals that  $\beta$ OHB reduces P62 expression, enhances the expression of PINK1 and Parkin, and elevates the LC3B I/II ratio, indicating the restoration of mitophagy. In summary, our research findings demonstrate that TBHP induces mitochondrial dysfunction and that  $\beta$ OHB restores mitophagy in an HCAR2-dependent manner.

AMPK plays a crucial role in regulating cellular energy balance by promoting ATP production and inhibiting ATP consumption through the modulation of metabolic enzymes (Yao et al., 2023). Activation of the AMPK complex occurs when cellular energy levels are low, as indicated by the phosphorylation of Thr-172 in the  $\alpha$ -subunit. AMPK expression and AMPK $\alpha$  phosphorylation are highly expressed in healthy articular cartilage. However, a significant decrease in AMPK $\alpha$  phosphorylation at the T172 locus was observed in articular cartilage from OA patients and surgery-induced OA mice, suggesting that AMPK activation serves as a protective mechanism for articular cartilage (Petursson et al., 2013). The mechanisms underlying the reduction in AMPK expression and activation remain unclear (Yao et al., 2023). Previous studies have established a link between mitochondrial dysfunction in OA chondrocytes and aberrant AMPK activity (Wang et al., 2015). Our investigation revealed that treatment with TBHP decreased the phosphorylation of AMPK in chondrocytes, while an ACLT-induced OA rat model also resulted in reduced AMPK phosphorylation. This impairment in AMPK activity subsequently led to mitochondrial dysfunction, resulting in inadequate energy production and increased ROS generation (Petursson et al., 2013). Research has indicated that the upregulation of total and phosphorylated AMPK expression through metformin administration can mitigate inflammation and postpone the onset of OA (Feng et al., 2020; Li et al., 2020; Wang et al., 2020). Furthermore, AMPK activation triggers essential kinases that facilitate autophagy, and metformin treatment enhances the expression of LC3 in chondrocytes (Feng et al., 2020; Guo et al., 2022; Hwang et al., 2021). Our investigation illustrated that  $\beta$ OHB elevates the phosphorylation status of AMPK both in vitro and in vivo, stimulating mitophagy and subsequently mitigating damage to chondrocytes in OA.

Additionally, we investigated the potential mechanisms of mepenzolate bromide (an HCAR2 inhibitor), Compound C (an AMPK antagonist), and Mdivi-1 (a mitochondrial division inhibitor) in OA rat models. In our research, we observed that 200 mg/kg  $\beta$ OHB exhibited a capacity to impede the progression of OA in rats. However, the introduction of mepenzolate bromide, Compound C, and Mdivi-1 significantly diminished the effectiveness of  $\beta$ OHB supplementation. Furthermore, mepenzolate bromide hindered the activation of AMPK and PINK1 activation by  $\beta$ OHB, while Compound C and Mdivi-1 did not inhibit the upregulation of HCAR2 expression by  $\beta$ OHB. Compound C impeded the activation of PINK1 by  $\beta$ OHB, whereas Mdivi-1 did not suppress the activation of AMPK induced by  $\beta$ OHB. Our findings suggest that  $\beta$ OHB may exert chondroprotective effects through the HCAR2/AMPK/PINK1 axis in rats.

However, it is important to acknowledge several limitations in this study. Firstly, due to the unavailability of healthy human chondrocyte resources, we utilized chondrocytes from rats. Secondly, the etiology of OA is multifaceted, and various modalities such as TBHP, IL-1 $\beta$ , H<sub>2</sub>O<sub>2</sub>, continuous passaging, UV irradiation, hypoxia, mechanical overload, TGF- $\beta$ 1, and FGF have been employed to establish in vitro chondrocyte senescence models (Rim et al., 2020; Xie et al., 2021). Thirdly, only wild-type rats were used in this study. The utilization of HCAR2 knockout rats in future studies would enhance



the validation of  $\beta$ OHB as a therapeutic strategy. Nevertheless, the extent to which these models accurately represent the *in vivo* situation of OA remains unknown.

## 5 | CONCLUSION

The present study presents novel findings indicating that  $\beta$ OHB exhibits the ability to counteract TBHP-induced chondrocyte inflammation, oxidative stress, senescence, and apoptosis, while also facilitating mitophagy via the HCAR2/AMPK/PINK1/Parkin pathway. Furthermore, both KD and intraperitoneal administration of  $\beta$ OHB demonstrate the potential to impede the advancement of OA in rats. These encouraging results contribute fresh insights into the clinical application of KD and  $\beta$ OHB supplementation for the treatment of OA.

## AUTHOR CONTRIBUTIONS

**Huangming Zhuang:** conceptualization, writing—original draft. **Xunshan Ren:** methodology, writing—review and editing. **Yuelong Zhang:** formal analysis, validation. **Huajie Li:** methodology. **Panghu Zhou:** conceptualization, project administration, funding acquisition.

## ACKNOWLEDGEMENTS

The authors would like to thank Lina Zhou, Yingxia Jin, Yuan He and Qiong Ding (Central Laboratory, Renmin Hospital of Wuhan University) for their assistance. Thanks to the home-for-researchers website (<https://www.home-for-researchers.com/static/index.html#/>) for their service. The graphical abstract is created with [BioRender.com](https://biorender.com).

## FUNDING INFORMATION

This work was supported by the National Natural Science Foundation of China (No. 82372489), the Hubei Medical Youth Tip-Top Talent to Panghu Zhou (No. CZ2024020005-11), the Fundamental Research Funds for the Central Universities (No. 2042023kf0224), Wuhan University Education and Development Foundation (No. 2002330) and the Cross-Innovation Talent Program of Renmin Hospital of Wuhan University (No. JCRCFZ-2022-019).

## CONFLICT OF INTEREST STATEMENT

The authors have declared that no competing interest exists.

## DATA AVAILABILITY STATEMENT

Data available on request from the authors.

## ORCID

Panghu Zhou  <https://orcid.org/0000-0002-7020-4258>

## REFERENCES

Abboud, M., AlAnouti, F., Georgaki, E., & Papandreou, D. (2021). Effect of ketogenic diet on quality of life in adults with chronic disease: A systematic review of randomized controlled trials. *Nutrients*, 13(12), 4463. <https://doi.org/10.3390/nu13124463>

Ahmad, N., Ansari, M. Y., & Haqqi, T. M. (2020). Role of iNOS in osteoarthritis: Pathological and therapeutic aspects. *Journal of Cellular Physiology*, 235(10), 6366–6376. <https://doi.org/10.1002/jcp.29607>

Ansari, M. Y., Khan, N. M., Ahmad, I., & Haqqi, T. M. (2018). Parkin clearance of dysfunctional mitochondria regulates ROS levels and increases survival of human chondrocytes. *Osteoarthritis and Cartilage*, 26(8), 1087–1097. <https://doi.org/10.1016/j.joca.2017.07.020>

Arra, M., Swarnkar, G., Alippe, Y., Mbalaviele, G., & Abu-Amer, Y. (2022). IkappaB-zeta signaling promotes chondrocyte inflammatory phenotype, senescence, and erosive joint pathology. *Bone Research*, 10(1), 12. <https://doi.org/10.1038/s41413-021-00183-9>

Ashrafi, G., & Schwarz, T. L. (2013). The pathways of mitophagy for quality control and clearance of mitochondria. *Cell Death and Differentiation*, 20(1), 31–42. <https://doi.org/10.1038/cdd.2012.81>

Balsa, E., Soustek, M. S., Thomas, A., Cogliati, S., Garcia-Poyatos, C., Martin-Garcia, E., ... Puigserver, P. (2019). ER and nutrient stress promote assembly of respiratory chain supercomplexes through the PERK-eIF2alpha Axis. *Molecular Cell*, 74(5), 877–890. <https://doi.org/10.1016/j.molcel.2019.03.031>

Bannuru, R. R., Osani, M. C., Vaysbrot, E. E., Arden, N. K., Bennell, K., Bierma-Zeinstra, S. M. A., ... McAlindon, T. E. (2019). OARSI guidelines for the non-surgical management of knee, hip, and polyarticular osteoarthritis. *Osteoarthritis and Cartilage*, 27(11), 1578–1589. <https://doi.org/10.1016/j.joca.2019.06.011>

Bay-Jensen, A. C., Mobasher, A., Thudium, C. S., Kraus, V. B., & Karsdal, M. A. (2022). Blood and urine biomarkers in osteoarthritis—An update on cartilage associated type II collagen and aggrecan markers. *Current Opinion in Rheumatology*, 34(1), 54–60. <https://doi.org/10.1097/BOR.0000000000000845>

Blanco, F. J., & Rego-Perez, I. (2020). Mitochondrial DNA in osteoarthritis disease. *Clinical Rheumatology*, 39(11), 3255–3259. <https://doi.org/10.1007/s10067-020-05406-8>

Carretta, M. D., Barria, Y., Borquez, K., Urra, B., Rivera, A., Alarcon, P., & Burgos, R. A. (2020). Beta-hydroxybutyrate and hydroxycarboxylic acid receptor 2 agonists activate the AKT, ERK and AMPK pathways, which are involved in bovine neutrophil chemotaxis. *Scientific Reports*, 10(1), 12491. <https://doi.org/10.1038/s41598-020-69500-2>

Chen, H., Tu, M., Liu, S., Wen, Y., & Chen, L. (2023). Dendrobine alleviates cellular senescence and osteoarthritis via the ROS/NF- $\kappa$ B Axis. *International Journal of Molecular Sciences*, 24(3), 2365. <https://doi.org/10.3390/ijms24032365>

Chen, H., Wu, J., Wang, Z., Wu, Y., Wu, T., Wu, Y., Wang, M., Wang, S., Wang, X., Wang, J., Yu, H., Hu, Y., & Shang, S. (2021). Trends and patterns of knee osteoarthritis in China: A longitudinal study of 17.7 million adults from 2008 to 2017. *International Journal of Environmental Research and Public Health*, 18(16), 8864. <https://doi.org/10.3390/ijerph18168864>

Chen, P., Liu, X., Gu, C., Zhong, P., Song, N., Li, M., Dai, Z., Fang, X., Liu, Z., Zhang, J., Tang, R., Fan, S., & Lin, X. (2022). A plant-derived natural photosynthetic system for improving cell anabolism. *Nature*, 612(7940), 546–554. <https://doi.org/10.1038/s41586-022-05499-y>

Chen, Y., Lin, J., Chen, J., Huang, C., Zhang, Z., Wang, J., Wang, K., & Wang, X. (2020). Mfn2 is involved in intervertebral disc degeneration through autophagy modulation. *Osteoarthritis and Cartilage*, 28(3), 363–374. <https://doi.org/10.1016/j.joca.2019.12.009>

Chen, Y., Ouyang, X., Hoque, R., Garcia-Martinez, I., Yousaf, M. N., Tonack, S., Offermanns, S., Dubuquoy, L., Louvet, A., Mathurin, P., Massey, V., Schnabl, B., Bataller, R. A., & Mehal, W. Z. (2018). Beta-Hydroxybutyrate protects from alcohol-induced liver injury via a Hcar2-cAMP dependent pathway. *Journal of Hepatology*, 69(3), 687–696. <https://doi.org/10.1016/j.jhep.2018.04.004>



Coryell, P. R., Diekman, B. O., & Loeser, R. F. (2021). Mechanisms and therapeutic implications of cellular senescence in osteoarthritis. *Nature Reviews Rheumatology*, 17(1), 47–57. <https://doi.org/10.1038/s41584-020-00533-7>

Davies, C. M., Guilak, F., Weinberg, J. B., & Fermor, B. (2008). Reactive nitrogen and oxygen species in interleukin-1-mediated DNA damage associated with osteoarthritis. *Osteoarthritis and Cartilage*, 16(5), 624–630. <https://doi.org/10.1016/j.joca.2007.09.012>

Dhingra, R., & Kirshenbaum, L. A. (2015). Succinate dehydrogenase complex II activity obligatorily links mitochondrial reserve respiratory capacity to cell survival in cardiac myocytes. *Cell Death & Disease*, 6(10), e1956. <https://doi.org/10.1038/cddis.2015.310>

Dmitrieva-Posocco, O., Wong, A. C., Lundgren, P., Golos, A. M., Descamps, H. C., Dohnalova, L., Cramer, Z., Tian, Y., Yueh, B., Eskiocak, O., Egervari, G., Lan, Y., Liu, J., Fan, J., Kim, J., Madhu, B., Schneider, K. M., Khozaianova, S., Andreeva, N., ... Levy, M. (2022). Beta-Hydroxybutyrate suppresses colorectal cancer. *Nature*, 605(7908), 160–165. <https://doi.org/10.1038/s41586-022-04649-6>

Du, L., Xing, Z., Tao, B., Li, T., Yang, D., Li, W., Zheng, Y., Kuang, C., & Yang, Q. (2020). Both IDO1 and TDO contribute to the malignancy of gliomas via the Kyn-AhR-AQP4 signaling pathway. *Signal Transduction and Targeted Therapy*, 5(1), 10. <https://doi.org/10.1038/s41392-019-0103-4>

Dynka, D., Kowalcze, K., Charuta, A., & Paziewska, A. (2023). The ketogenic diet and cardiovascular diseases. *Nutrients*, 15(15), 3368. <https://doi.org/10.3390/nu15153368>

Effinger, D., Hirschberger, S., Yoncheva, P., Schmid, A., Heine, T., Newels, P., Schütz, B., Meng, C., Gigl, M., Kleigrewe, K., Holdt, L. M., Teupser, D., & Kreth, S. (2023). A ketogenic diet substantially reshapes the human metabolome. *Clinical Nutrition*, 42, 1202–1212. <https://doi.org/10.1016/j.clnu.2023.04.027>

Eskandari, E., & Eaves, C. J. (2022). Paradoxical roles of caspase-3 in regulating cell survival, proliferation, and tumorigenesis. *The Journal of Cell Biology*, 221(6), e202201159. <https://doi.org/10.1083/jcb.202201159>

Eyre, D. (2002). Collagen of articular cartilage. *Arthritis Research*, 4(1), 30–35. <https://doi.org/10.1186/ar380>

Feng, X., Pan, J., Li, J., Zeng, C., Qi, W., Shao, Y., Liu, X., Liu, L., Xiao, G., Zhang, H., Bai, X., & Cai, D. (2020). Metformin attenuates cartilage degeneration in an experimental osteoarthritis model by regulating AMPK/mTOR. *Aging (Albany NY)*, 12(2), 1087–1103. <https://doi.org/10.18632/aging.102635>

Fernandez-Moreno, M., Rego-Perez, I., & Blanco, F. J. (2022). Is osteoarthritis a mitochondrial disease? What is the evidence. *Current Opinion in Rheumatology*, 34(1), 46–53. <https://doi.org/10.1097/BOR.00000000000000855>

Ferrer, M., Mourikis, N., Davidson, E. E., Kleeman, S. O., Zaccaria, M., Habel, J., & Janowitz, T. (2023). Ketogenic diet promotes tumor ferroptosis but induces relative corticosterone deficiency that accelerates cachexia. *Cell Metabolism*, 35(7), 1147–1162 e1147. <https://doi.org/10.1016/j.cmet.2023.05.008>

Fu, S. P., Li, S. N., Wang, J. F., Li, Y., Xie, S. S., Xue, W. J., Huang, B. X., Lv, Q. K., Lei, L. C., Liu, G. W., Wang, W., & Liu, J. X. (2014). BHBA suppresses LPS-induced inflammation in BV-2 cells by inhibiting NF-κB activation. *Mediators of Inflammation*, 2014, 983401. <https://doi.org/10.1155/2014/983401>

Geisler, S., Holmstrom, K. M., Skujat, D., Fiesel, F. C., Rothfuss, O. C., Kahle, P. J., & Springer, W. (2010). PINK1/Parkin-mediated mitophagy is dependent on VDAC1 and p62/SQSTM1. *Nature Cell Biology*, 12(2), 119–131. <https://doi.org/10.1038/ncb2012>

Gong, Y., Tang, N., Liu, P., Sun, Y., Lu, S., Liu, W., Tan, L., Song, C., Qiu, X., Liao, Y., Yu, S., Liu, X., Lin, S. H., & Ding, C. (2022). Newcastle disease virus degrades SIRT3 via PINK1-PRKN-dependent mitophagy to reprogram energy metabolism in infected cells. *Autophagy*, 18(7), 1503–1521. <https://doi.org/10.1080/15548627.2021.1990515>

Gorini, S., Armani, A., & Caprio, M. (2023). Very low-calorie ketogenic diet: A valuable and fashionable nutritional therapy. When could it become dangerous? *Diabetes/Metabolism Research and Reviews*, 39(8), e3698. <https://doi.org/10.1002/dmrr.3698>

Goutas, A., Syrrou, C., Papathanasiou, I., Tseou, A., & Trachana, V. (2018). The autophagic response to oxidative stress in osteoarthritic chondrocytes is deregulated. *Free Radical Biology & Medicine*, 126, 122–132. <https://doi.org/10.1016/j.freeradbiomed.2018.08.003>

Guilak, F., Nims, R. J., Dicks, A., Wu, C. L., & Meulenbelt, I. (2018). Osteoarthritis as a disease of the cartilage pericellular matrix. *Matrix Biology*, 71–72, 40–50. <https://doi.org/10.1016/j.matbio.2018.05.008>

Guo, H., Ouyang, Y., Yin, H., Cui, H., Deng, H., Liu, H., Jian, Z., Fang, J., Zuo, Z., Wang, X., Zhao, L., Zhu, Y., Geng, Y., & Ouyang, P. (2022). Induction of autophagy via the ROS-dependent AMPK-mTOR pathway protects copper-induced spermatogenesis disorder. *Redox Biology*, 49, 102227. <https://doi.org/10.1016/j.redox.2021.102227>

Han, Y. C., Tang, S. Q., Liu, Y. T., Li, A. M., Zhan, M., Yang, M., Song, N., Zhang, W., Wu, X. Q., Peng, C. H., Zhang, H., & Yang, S. (2021). AMPK agonist alleviate renal tubulointerstitial fibrosis via activating mitophagy in high fat and streptozotocin induced diabetic mice. *Cell Death & Disease*, 12(10), 925. <https://doi.org/10.1038/s41419-021-04184-8>

Hardie, D. G., Ross, F. A., & Hawley, S. A. (2012). AMPK: A nutrient and energy sensor that maintains energy homeostasis. *Nature Reviews Molecular Cell Biology*, 13(4), 251–262. <https://doi.org/10.1038/nrm3311>

He, Q., Lin, Y., Chen, B., Chen, C., Zeng, J., Dou, X., Cai, D., Zhou, C., & Wang, H. (2024). Vitamin K2 ameliorates osteoarthritis by suppressing ferroptosis and extracellular matrix degradation through activation GPX4's dual functions. *Biomedicine & Pharmacotherapy*, 175, 116697. <https://doi.org/10.1016/j.biopha.2024.116697>

Heinegard, D., & Saxne, T. (2011). The role of the cartilage matrix in osteoarthritis. *Nature Reviews Rheumatology*, 7(1), 50–56. <https://doi.org/10.1038/nrrheum.2010.198>

Hinge, A., He, J., Bartram, J., Javier, J., Xu, J., Fjellman, E., Sesaki, H., Li, T., Yu, J., Wunderlich, M., Mulloy, J., Kofron, M., Salomonis, N., Grimes, H. L., & Filippi, M. D. (2020). Asymmetrically segregated mitochondria provide cellular memory of hematopoietic stem cell replicative history and drive HSC attrition. *Cell Stem Cell*, 26(3), 420–430. <https://doi.org/10.1016/j.stem.2020.01.016>

Huang, W., Hickson, L. J., Eirin, A., Kirkland, J. L., & Lerman, L. O. (2022). Cellular senescence: The good, the bad and the unknown. *Nature Reviews Nephrology*, 18(10), 611–627. <https://doi.org/10.1038/s41581-022-00601-z>

Huang, Y., Kwan, K. K. L., Leung, K. W., Yao, P., Wang, H., Dong, T. T., & Tsim, K. W. K. (2019). Ginseng extracts modulate mitochondrial bioenergetics of live cardiomyoblasts: A functional comparison of different extraction solvents. *Journal of Ginseng Research*, 43(4), 517–526. <https://doi.org/10.1016/j.jgr.2018.02.002>

Hunter, D. J., & Bierma-Zeinstra, S. (2019). Osteoarthritis. *Lancet*, 393(10182), 1745–1759. [https://doi.org/10.1016/S0140-6736\(19\)30417-9](https://doi.org/10.1016/S0140-6736(19)30417-9)

Hwang, H. Y., Shim, J. S., Kim, D., & Kwon, H. J. (2021). Antidepressant drug sertraline modulates AMPK-MTOR signaling-mediated autophagy via targeting mitochondrial VDAC1 protein. *Autophagy*, 17(10), 2783–2799. <https://doi.org/10.1080/15548627.2020.1841953>

Inada, M., Wang, Y., Byrne, M. H., Rahman, M. U., Miyaura, C., Lopez-Otin, C., & Krane, S. M. (2004). Critical roles for collagenase-3 (Mmp13) in development of growth plate cartilage and in endochondral ossification. *Proceedings of the National Academy of Sciences of the United States of America*, 101(49), 17192–17197. <https://doi.org/10.1073/pnas.0407788101>

Jeon, O. H., David, N., Campisi, J., & Elisseeff, J. H. (2018). Senescent cells and osteoarthritis: A painful connection. *The Journal of Clinical Investigation*, 128(4), 1229–1237. <https://doi.org/10.1172/JCI95147>



Ji, L., He, Q., Liu, Y., Deng, Y., Xie, M., Luo, K., & Li, T. (2022). Ketone body beta-Hydroxybutyrate prevents myocardial oxidative stress in septic cardiomyopathy. *Oxidative Medicine and Cellular Longevity*, 2022, 2513837. <https://doi.org/10.1155/2022/2513837>

Jiang, N., Xing, B., Peng, R., Shang, J., Wu, B., Xiao, P., & Lu, H. (2022). Inhibition of Cpt1a alleviates oxidative stress-induced chondrocyte senescence via regulating mitochondrial dysfunction and activating mitophagy. *Mechanisms of Ageing and Development*, 205, 111688. <https://doi.org/10.1016/j.mad.2022.111688>

Jin, Y., Liu, Z., Li, Z., Li, H., Zhu, C., Li, R., & Fang, B. (2022). Histone demethylase JMJD3 downregulation protects against aberrant force-induced osteoarthritis through epigenetic control of NR4A1. *International Journal of Oral Science*, 14(1), 34. <https://doi.org/10.1038/s41368-022-00190-4>

Kawakami, R., Sunaga, H., Iso, T., Kaneko, R., Koitabashi, N., Obokata, M., Harada, T., Matsui, H., Yokoyama, T., & Kurabayashi, M. (2022). Ketone body and FGF21 coordinately regulate fasting-induced oxidative stress response in the heart. *Scientific Reports*, 12(1), 7338. <https://doi.org/10.1038/s41598-022-10993-4>

Kaye, D. M., Shihata, W. A., Jama, H. A., Tsyanov, K., Ziemann, M., Kiriazis, H., ... Marques, F. Z. (2020). Deficiency of prebiotic fiber and insufficient signaling through gut metabolite-sensing receptors leads to cardiovascular disease. *Circulation*, 141(17), 1393-1403. <https://doi.org/10.1161/CIRCULATIONAHA.119.043081>

Kiani, C., Chen, L., Wu, Y. J., Yee, A. J., & Yang, B. B. (2002). Structure and function of aggrecan. *Cell Research*, 12(1), 19-32. <https://doi.org/10.1038/sj.cr.7290106>

Konig, T., Nolte, H., Aaltonen, M. J., Tatsuta, T., Krosl, M., Stroh, T., & McBride, H. M. (2021). MIROs and DRP1 drive mitochondrial-derived vesicle biogenesis and promote quality control. *Nature Cell Biology*, 23(12), 1271-1286. <https://doi.org/10.1038/s41556-021-00798-4>

Koyano, F., Okatsu, K., Kosako, H., Tamura, Y., Go, E., Kimura, M., & Matsuda, N. (2014). Ubiquitin is phosphorylated by PINK1 to activate parkin. *Nature*, 510(7503), 162-166. <https://doi.org/10.1038/nature13392>

Lee, A. K., Kim, D. H., Bang, E., Choi, Y. J., & Chung, H. Y. (2020). Beta-Hydroxybutyrate suppresses lipid accumulation in aged liver through GPR109A-mediated signaling. *Aging and Disease*, 11(4), 777-790. <https://doi.org/10.14336/AD.2019.0926>

Li, J., Zhang, B., Liu, W. X., Lu, K., Pan, H., Wang, T., & Chen, D. (2020). Metformin limits osteoarthritis development and progression through activation of AMPK signalling. *Annals of the Rheumatic Diseases*, 79(5), 635-645. <https://doi.org/10.1136/annrheumdis-2019-216713>

Liu, L., Zhang, W., Liu, T., Tan, Y., Chen, C., Zhao, J., & Ma, C. (2023). The physiological metabolite alpha-ketoglutarate ameliorates osteoarthritis by regulating mitophagy and oxidative stress. *Redox Biology*, 62, 102663. <https://doi.org/10.1016/j.redox.2023.102663>

Liu, Z., Li, W., Geng, L., Sun, L., Wang, Q., Yu, Y., & Liu, G. H. (2022). Cross-species metabolomic analysis identifies uridine as a potent regeneration promoting factor. *Cell Discovery*, 8(1), 6. <https://doi.org/10.1038/s41421-021-00361-3>

Lopez-Otin, C., Blasco, M. A., Partridge, L., Serrano, M., & Kroemer, G. (2023). Hallmarks of aging: An expanding universe. *Cell*, 186(2), 243-278. <https://doi.org/10.1016/j.cell.2022.11.001>

Lu, H., Jia, C., Wu, D., Jin, H., Lin, Z., Pan, J., Li, X., & Wang, W. (2021). Fibroblast growth factor 21 (FGF21) alleviates senescence, apoptosis, and extracellular matrix degradation in osteoarthritis via the SIRT1-mTOR signaling pathway. *Cell Death & Disease*, 12(10), 865. <https://doi.org/10.1038/s41419-021-04157-x>

Luda, K. M., Longo, J., Kitchen-Goosen, S. M., Duimstra, L. R., Ma, E. H., Watson, M. J., Oswald, B. M., Fu, Z., Madaj, Z., Kupai, A., Dickson, B. M., DeCamp, L. M., Dahabieh, M. S., Compton, S. E., Teis, R., Kaymak, I., Lau, K. H., Kelly, D. P., Puchalska, P., ... Jones, R. G. (2023). Ketolysis drives CD8<sup>+</sup> T cell effector function through effects on histone acetylation. *Immunity*, 56(9), 2021-2035. <https://doi.org/10.1016/j.immuni.2023.07.002>

Luo, S., Yang, M., Han, Y., Zhao, H., Jiang, N., Li, L., Chen, W., Li, C., Yang, J., Liu, Y., Liu, C., Zhao, C., & Sun, L. (2022). Beta-Hydroxybutyrate against cisplatin-induced acute kidney injury via inhibiting NLRP3 inflammasome and oxidative stress. *International Immunopharmacology*, 111, 109101. <https://doi.org/10.1016/j.intimp.2022.109101>

Lv, Z., Han, J., Li, J., Guo, H., Fei, Y., Sun, Z., Dong, J., Wang, M., Fan, C., Li, W., Xie, Y., Sun, W., Chen, J., Liu, Y., Chen, F., Liu, Z., Liu, A., Wu, R., Xu, X., ... Shi, D. (2022). Single cell RNA-seq analysis identifies ferroptotic chondrocyte cluster and reveals TRPV1 as an anti-ferroptotic target in osteoarthritis. *eBioMedicine*, 84, 104258. <https://doi.org/10.1016/j.ebiom.2022.104258>

Mao, C., Gao, M., Zang, S. K., Zhu, Y., Shen, D. D., Chen, L. N., Yang, L., Wang, Z., Zhang, H., Wang, W. W., Shen, Q., Lu, Y., Ma, X., & Zhang, Y. (2023). Orthosteric and allosteric modulation of human HCAR2 signalling complex. *Nature Communications*, 14(1), 7620. <https://doi.org/10.1038/s41467-023-43537-z>

Matsuda, N., Sato, S., Shiba, K., Okatsu, K., Saisho, K., Gautier, C. A., Sou, Y. S., Saiki, S., Kawajiri, S., Sato, F., Kimura, M., Komatsu, M., Hattori, N., & Tanaka, K. (2010). PINK1 stabilized by mitochondrial depolarization recruits Parkin to damaged mitochondria and activates latent Parkin for mitophagy. *The Journal of Cell Biology*, 189(2), 211-221. <https://doi.org/10.1083/jcb.200910140>

Mickiewicz, B., Kelly, J. J., Ludwig, T. E., Weljie, A. M., Wiley, J. P., Schmidt, T. A., & Vogel, H. J. (2015). Metabolic analysis of knee synovial fluid as a potential diagnostic approach for osteoarthritis. *Journal of Orthopaedic Research*, 33(11), 1631-1638. <https://doi.org/10.1002/jor.22949>

Milner, P. I., Fairfax, T. P., Browning, J. A., Wilkins, R. J., & Gibson, J. S. (2006). The effect of O<sub>2</sub> tension on pH homeostasis in equine articular chondrocytes. *Arthritis and Rheumatism*, 54(11), 3523-3532. <https://doi.org/10.1002/art.22209>

Miyauchi, T., Uchida, Y., Kadono, K., Hirao, H., Kawasoe, J., Watanabe, T., & Uemoto, S. (2019). Up-regulation of FOXO1 and reduced inflammation by beta-hydroxybutyric acid are essential diet restriction benefits against liver injury. *Proceedings of the National Academy of Sciences of the United States of America*, 116(27), 13533-13542. <https://doi.org/10.1073/pnas.1820282116>

Moutinho, M., Puntambekar, S. S., Tsai, A. P., Coronel, I., Lin, P. B., Casali, B. T., ... Landreth, G. E. (2022). The niacin receptor HCAR2 modulates microglial response and limits disease progression in a mouse model of Alzheimer's disease. *Science Translational Medicine*, 14(637), eabl7634. <https://doi.org/10.1126/scitranslmed.abl7634>

Nasui, B. A., Talaba, P., Nasui, G. A., Sirbu, D. M., Borda, I. M., Pop, A. L., & Ungur, R. A. (2022). The influence of diet and physical activity on oxidative stress in Romanian females with osteoarthritis. *Nutrients*, 14(19), 4159. <https://doi.org/10.3390/nu14194159>

Newman, J. C., & Verdin, E. (2014). Ketone bodies as signaling metabolites. *Trends in Endocrinology and Metabolism*, 25(1), 42-52. <https://doi.org/10.1016/j.tem.2013.09.002>

Niu, K., Fang, H., Chen, Z., Zhu, Y., Tan, Q., Wei, D., & Zhao, Y. (2020). USP33 deubiquitinates PRKN/parkin and antagonizes its role in mitophagy. *Autophagy*, 16(4), 724-734. <https://doi.org/10.1080/15548627.2019.1656957>

O'Neill, T. W., McCabe, P. S., & McBeth, J. (2018). Update on the epidemiology, risk factors and disease outcomes of osteoarthritis. *Best Practice & Research. Clinical Rheumatology*, 32(2), 312-326. <https://doi.org/10.1016/j.berh.2018.10.007>

Onishi, M., Yamano, K., Sato, M., Matsuda, N., & Okamoto, K. (2021). Molecular mechanisms and physiological functions of mitophagy. *The EMBO Journal*, 40(3), e104705. <https://doi.org/10.15252/embj.2020104705>



Palikaras, K., Daskalaki, I., Markaki, M., & Tavernarakis, N. (2017). Mitophagy and age-related pathologies: Development of new therapeutics by targeting mitochondrial turnover. *Pharmacology & Therapeutics*, 178, 157–174. <https://doi.org/10.1016/j.pharmthera.2017.04.005>

Pan, Y. N., Jia, C., Yu, J. P., Wu, Z. W., Xu, G. C., & Huang, Y. X. (2023). Fibroblast growth factor 9 reduces TBHP-induced oxidative stress in chondrocytes and diminishes mouse osteoarthritis by activating ERK/Nrf2 signaling pathway. *International Immunopharmacology*, 114, 109606. <https://doi.org/10.1016/j.intimp.2022.109606>

Petursson, F., Husa, M., June, R., Lotz, M., Terkeltaub, R., & Liu-Bryan, R. (2013). Linked decreases in liver kinase B1 and AMP-activated protein kinase activity modulate matrix catabolic responses to biomechanical injury in chondrocytes. *Arthritis Research & Therapy*, 15(4), R77. <https://doi.org/10.1186/ar4254>

Pritzker, K. P., Gay, S., Jimenez, S. A., Ostergaard, K., Pelletier, J. P., Revell, P. A., Salter, D., & van den Berg, W. B. (2006). Osteoarthritis cartilage histopathology: Grading and staging. *Osteoarthritis and Cartilage*, 14(1), 13–29. <https://doi.org/10.1016/j.joca.2005.07.014>

Puchalska, P., & Crawford, P. A. (2017). Multi-dimensional roles of ketone bodies in fuel metabolism, signaling, and therapeutics. *Cell Metabolism*, 25(2), 262–284. <https://doi.org/10.1016/j.cmet.2016.12.022>

Puchalska, P., & Crawford, P. A. (2021). Metabolic and signaling roles of ketone bodies in health and disease. *Annual Review of Nutrition*, 41, 49–77. <https://doi.org/10.1146/annurev-nutr-111120-111518>

Rahman, M., Muhammad, S., Khan, M. A., Chen, H., Ridder, D. A., Muller-Fielitz, H., ... Schwaninger, M. (2014). The beta-hydroxybutyrate receptor HCA2 activates a neuroprotective subset of macrophages. *Nature Communications*, 5, 3944. <https://doi.org/10.1038/ncomms4944>

Rim, Y. A., Nam, Y., & Ju, J. H. (2020). The role of chondrocyte hypertrophy and senescence in osteoarthritis initiation and progression. *International Journal of Molecular Sciences*, 21(7), 2358. <https://doi.org/10.3390/ijms21072358>

Santoro, A., Conde, J., Scottece, M., Abella, V., Lopez, V., Pino, J., Gómez, R., Gómez-Reino, J. J., & Gualillo, O. (2015). Choosing the right chondrocyte cell line: Focus on nitric oxide. *Journal of Orthopaedic Research*, 33(12), 1784–1788. <https://doi.org/10.1002/jor.22954>

Shang, J., Lin, N., Peng, R., Jiang, N., Wu, B., Xing, B., Lin, S., Xu, X., & Lu, H. (2023). Inhibition of Klf10 attenuates oxidative stress-induced senescence of chondrocytes via modulating mitophagy. *Molecules*, 28(3), 924. <https://doi.org/10.3390/molecules28030924>

Sharma, R., & Ramanathan, A. (2020). The aging metabolome-biomarkers to hub metabolites. *Proteomics*, 20(5–6), e1800407. <https://doi.org/10.1002/pmic.201800407>

Shimazu, T., Hirshey, M. D., Newman, J., He, W., Shirakawa, K., Le Moan, N., Grueter, C. A., Lim, H., Saunders, L. R., Stevens, R. D., Newgard, C. B., Farese, R. V., Jr., de Cabo, R., Ulrich, S., Akassoglou, K., & Verdin, E. (2013). Suppression of oxidative stress by beta-hydroxybutyrate, an endogenous histone deacetylase inhibitor. *Science*, 339(6116), 211–214. <https://doi.org/10.1126/science.1227166>

Shimomura, S., Inoue, H., Arai, Y., Nakagawa, S., Fujii, Y., Kishida, T., ... Kubo, T. (2022). Hypoxia promotes differentiation of pure cartilage from human induced pluripotent stem cells. *Molecular Medicine Reports*, 26(1), 229. <https://doi.org/10.3892/mmr.2022.12745>

Shin, H. J., Park, H., Shin, N., Kwon, H. H., Yin, Y., Hwang, J. A., Song, H. J., Kim, J., Kim, D. W., & Beom, J. (2019). Pink1-mediated chondrocytic Mitophagy contributes to cartilage degeneration in osteoarthritis. *Journal of Clinical Medicine*, 8(11), 1849. <https://doi.org/10.3390/jcm8111849>

Singh, N., Gurav, A., Sivaprakasam, S., Brady, E., Padia, R., Shi, H., Thangaraju, M., Prasad, P. D., & Ganapathy, V. (2014). Activation of Gpr109a, receptor for niacin and the commensal metabolite butyrate, suppresses colonic inflammation and carcinogenesis. *Immunity*, 40(1), 128–139. <https://doi.org/10.1016/j.jimmuni.2013.12.007>

Stefan, M., Sharp, M., Gheith, R., Lowery, R., & Wilson, J. (2021). The effect of exogenous Beta-Hydroxybutyrate salt supplementation on metrics of safety and health in adolescents. *Nutrients*, 13(3), 854. <https://doi.org/10.3390/nu13030854>

Suen, D. F., Narendra, D. P., Tanaka, A., Manfredi, G., & Youle, R. J. (2010). Parkin overexpression selects against a deleterious mtDNA mutation in heteroplasmic cybrid cells. *Proceedings of the National Academy of Sciences of the United States of America*, 107(26), 11835–11840. <https://doi.org/10.1073/pnas.0914569107>

Sun, K., Jing, X., Guo, J., Yao, X., & Guo, F. (2021). Mitophagy in degenerative joint diseases. *Autophagy*, 17(9), 2082–2092. <https://doi.org/10.1080/15548627.2020.1822097>

Sun, X., Shu, Y., Ye, G., Wu, C., Xu, M., Gao, R., Huang, D., & Zhang, J. (2022). Histone deacetylase inhibitors inhibit cervical cancer growth through Parkin acetylation-mediated mitophagy. *Acta Pharmaceutica Sinica B*, 12(2), 838–852. <https://doi.org/10.1016/j.apsb.2021.07.003>

Tao, S., Yang, T., Yin, Y., & Zhang, Q. (2024). Mitochondrial reactive oxygen species promote mitochondrial damage in high glucose-induced dysfunction and apoptosis of human dental pulp cells. *Journal of Dental Sciences*, 19(1), 292–302. <https://doi.org/10.1016/j.jds.2023.04.008>

Tran, M. T., Zsengeller, Z. K., Berg, A. H., Khankin, E. V., Bhasin, M. K., Kim, W., Clish, C. B., Stillman, I. E., Karumanchi, S. A., Rhee, E. P., & Parikh, S. M. (2016). PGC1alpha drives NAD biosynthesis linking oxidative metabolism to renal protection. *Nature*, 531(7595), 528–532. <https://doi.org/10.1038/nature17184>

Tsuchida, A. I., Beekhuizen, M., t Hart, M. C., Radstake, T. R., Dhert, W. J., Saris, D. B., ... Creemers, L. B. (2014). Cytokine profiles in the joint depend on pathology, but are different between synovial fluid, cartilage tissue and cultured chondrocytes. *Arthritis Research & Therapy*, 16(5), 441. <https://doi.org/10.1186/s13075-014-0441-0>

Walters, R. W., Shukla, A. K., Kovacs, J. J., Violin, J. D., DeWire, S. M., Lam, C. M., & Lefkowitz, R. J. (2009). Beta-Arrestin1 mediates nicotinic acid-induced flushing, but not its antilipolytic effect, in mice. *The Journal of Clinical Investigation*, 119(5), 1312–1321. <https://doi.org/10.1172/JCI36806>

Wang, C., Yang, Y., Zhang, Y., Liu, J., Yao, Z., & Zhang, C. (2019). Protective effects of metformin against osteoarthritis through upregulation of SIRT3-mediated PINK1/Parkin-dependent mitophagy in primary chondrocytes. *Bioscience Trends*, 12(6), 605–612. <https://doi.org/10.5582/bst.2018.01263>

Wang, C., Yao, Z., Zhang, Y., Yang, Y., Liu, J., Shi, Y., & Zhang, C. (2020). Metformin mitigates cartilage degradation by activating AMPK/SIRT1-mediated autophagy in a mouse osteoarthritis model. *Frontiers in Pharmacology*, 11, 1114. <https://doi.org/10.3389/fphar.2020.01114>

Wang, Y., Zhao, X., Lotz, M., Terkeltaub, R., & Liu-Bryan, R. (2015). Mitochondrial biogenesis is impaired in osteoarthritis chondrocytes but reversible via peroxisome proliferator-activated receptor gamma coactivator 1α. *Arthritis & Rheumatology*, 67(8), 2141–2153. <https://doi.org/10.1002/art.39182>

Xie, J., Wang, Y., Lu, L., Liu, L., Yu, X., & Pei, F. (2021). Cellular senescence in knee osteoarthritis: Molecular mechanisms and therapeutic implications. *Ageing Research Reviews*, 70, 101413. <https://doi.org/10.1016/j.arr.2021.101413>

Xu, L., Wu, Z., He, Y., Chen, Z., Xu, K., Yu, W., Fang, W., Ma, C., Moqbel, S. A. A., Ran, J., Xiong, Y., & Wu, L. (2020). MFN2 contributes to metabolic disorders and inflammation in the aging of rat chondrocytes and osteoarthritis. *Osteoarthritis and Cartilage*, 28(8), 1079–1091. <https://doi.org/10.1016/j.joca.2019.11.011>

Yamano, K., & Youle, R. J. (2013). PINK1 is degraded through the N-end rule pathway. *Autophagy*, 9(11), 1758–1769. <https://doi.org/10.4161/auto.24633>

Yao, Q., Wu, X., Tao, C., Gong, W., Chen, M., Qu, M., Zhong, Y., He, T., Chen, S., & Xiao, G. (2023). Osteoarthritis: Pathogenic signaling



pathways and therapeutic targets. *Signal Transduction and Targeted Therapy*, 8(1), 56. <https://doi.org/10.1038/s41392-023-01330-w>

Youle, R. J., & Narendra, D. P. (2011). Mechanisms of mitophagy. *Nature Reviews Molecular Cell Biology*, 12(1), 9–14. <https://doi.org/10.1038/nrm3028>

Youm, Y. H., Nguyen, K. Y., Grant, R. W., Goldberg, E. L., Bodogai, M., Kim, D., Planavsky, N., Lupfer, C., Kanneganti, T. D., Kang, S., Horvath, T. L., Fahmy, T. M., Crawford, P. A., Biragyn, A., Alnemri, E., & Dixit, V. D. (2015). The ketone metabolite beta-hydroxybutyrate blocks NLRP3 inflammasome-mediated inflammatory disease. *Nature Medicine*, 21(3), 263–269. <https://doi.org/10.1038/nm.3804>

Yu, H., Liu, Y., Yang, X., He, J., Zhang, F., Zhong, Q., & Guo, X. (2021). Strontium ranelate promotes chondrogenesis through inhibition of the Wnt/beta-catenin pathway. *Stem Cell Research & Therapy*, 12(1), 296. <https://doi.org/10.1186/s13287-021-02372-z>

Yu, P. B., Hong, C. C., Sachidanandan, C., Babitt, J. L., Deng, D. Y., Hoyng, S. A., Lin, H. Y., Bloch, K. D., & Peterson, R. T. (2008). Dorsomorphin inhibits BMP signals required for embryogenesis and iron metabolism. *Nature Chemical Biology*, 4(1), 33–41. <https://doi.org/10.1038/nchembio.2007.54>

Zhang, M., Zhou, Q., Liang, Q. Q., Li, C. G., Holz, J. D., Tang, D., Sheu, T. J., Li, T. F., Shi, Q., & Wang, Y. J. (2009). IGF-1 regulation of type II collagen and MMP-13 expression in rat endplate chondrocytes via distinct signaling pathways. *Osteoarthritis and Cartilage*, 17(1), 100–106. <https://doi.org/10.1016/j.joca.2008.05.007>

Zhang, S. J., Li, Z. H., Zhang, Y. D., Chen, J., Li, Y., Wu, F. Q., Wang, W., Cui, Z. J., & Chen, G. Q. (2021). Ketone body 3-Hydroxybutyrate ameliorates atherosclerosis via receptor Gpr109a-mediated calcium influx. *Advance Sciences (Weinh)*, 8(9), 2003410. <https://doi.org/10.1002/advs.202003410>

Zhang, Y., Jin, W., Chen, J., Wei, S., Cai, W., Zhong, Y., Zhou, Y., & Peng, H. (2023). Gastrodin alleviates rat chondrocyte senescence and mitochondrial dysfunction through Sirt3. *International Immunopharmacology*, 118, 110022. <https://doi.org/10.1016/j.intimp.2023.110022>

Zhao, C., Wang, H., Liu, Y., Cheng, L., Wang, B., Tian, X., Fu, H., Wu, C., Li, Z., Shen, C., Yu, J., Yang, S., Hu, H., Fu, P., Ma, L., Wang, C., Yan, W., & Shao, Z. (2023). Biased allosteric activation of ketone body receptor HCAR2 suppresses inflammation. *Molecular Cell*, 83, 3171–3187.e7. <https://doi.org/10.1016/j.molcel.2023.07.030>

Zheng, L., Zhang, Z., Sheng, P., & Mobasher, A. (2021). The role of metabolism in chondrocyte dysfunction and the progression of osteoarthritis. *Ageing Research Reviews*, 66, 101249. <https://doi.org/10.1016/j.arr.2020.101249>

Zhuang, C., Wang, Y., Zhang, Y., & Xu, N. (2018). Oxidative stress in osteoarthritis and antioxidant effect of polysaccharide from angelica sinensis. *International Journal of Biological Macromolecules*, 115, 281–286. <https://doi.org/10.1016/j.ijbiomac.2018.04.083>

## SUPPORTING INFORMATION

Additional supporting information can be found online in the Supporting Information section at the end of this article.

**How to cite this article:** Zhuang, H., Ren, X., Zhang, Y., Li, H., & Zhou, P. (2024).  $\beta$ -Hydroxybutyrate enhances chondrocyte mitophagy and reduces cartilage degeneration in osteoarthritis via the HCAR2/AMPK/PINK1/Parkin pathway. *Aging Cell*, 23, e14294. <https://doi.org/10.1111/ace.14294>